CHALMERS
UNIVERSITY OF TECHNOLOGY

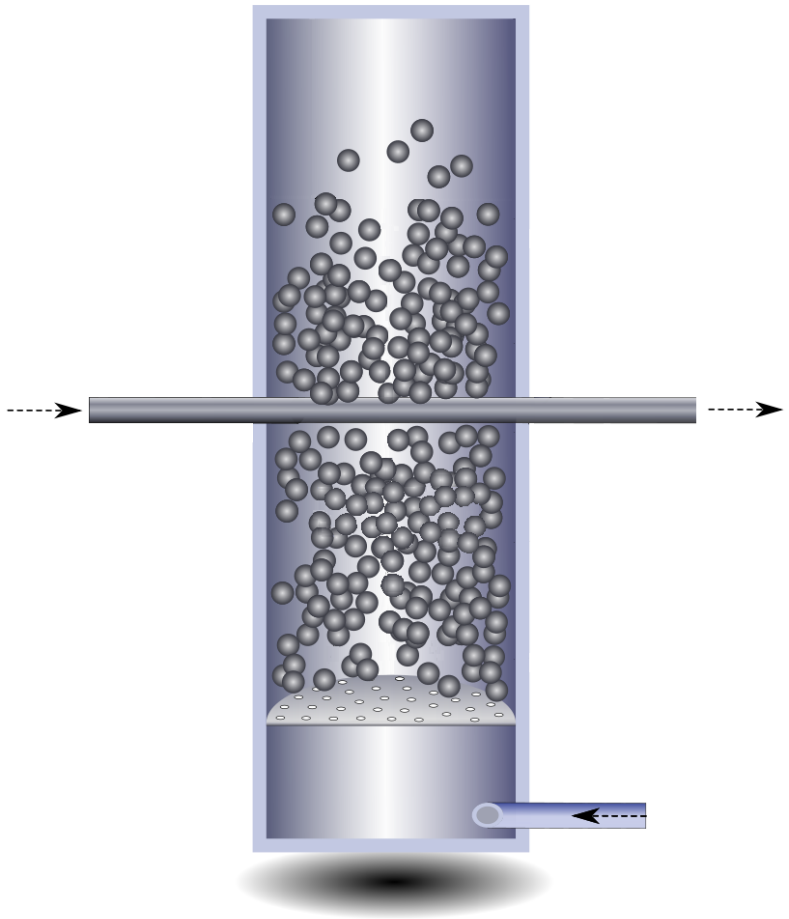

Determination of heat transfer coefficient to tube submerged in bubbling fluidized bed reactor

Master's thesis in Sustainable Energy Systems

VIKTOR SKÖLDBERG
LOVISA ÖHRBY

Department of Space, Earth and Environment
CHALMERS UNIVERSITY OF TECHNOLOGY
Gothenburg, Sweden 2018

Master's thesis 2018

Determination of heat transfer coefficient to tube submerged in bubbling fluidized bed reactor

VIKTOR SKÖLDBERG
LOVISA ÖHRBY

CHALMERS
UNIVERSITY OF TECHNOLOGY

Department of Space, Earth and Environment
Division of Energy Technology
Chalmers University of Technology
Gothenburg, Sweden 2018

Determination of heat transfer coefficient to tube submerged in bubbling fluidized bed reactor
VIKTOR SKÖLDBERG, LOVISA ÖHRBY

© VIKTOR SKÖLDBERG, LOVISA ÖHRBY, 2018.

Supervisor: Viktor Stenberg, Department of Space, Earth and Environment
Examiner: Magnus Rydén, Department of Space, Earth and Environment

Master's Thesis 2018
Department of Space, Earth and Environment
Division of Energy Technology
Chalmers University of Technology
SE-412 96 Gothenburg
Telephone +46 31 772 1000

Cover: Illustration of the lab-scale fluidized bed reactor and the submerged tube.

Typeset in LaTeX
Printed by Chalmers Reproservice
Gothenburg, Sweden 2018

Determination of heat transfer coefficient to tube submerged in bubbling fluidized bed reactor

VIKTOR SKÖLDBERG, LOVISA ÖHRBY
Department of Space, Earth and Environment
Chalmers University of Technology

Abstract

Hydrogen is an important raw material in refineries and chemical industries, representing around 2% of the world's primary energy demand. Today, the most important method for hydrogen production is steam reforming of natural gas. The steam reforming reaction is strongly endothermic and requires high temperatures (around 800-950°C) to proceed. The heat transfer to the reforming is conventionally done with radiative furnaces with flame temperatures of around 1500°C. A suggested method to improve the heat transfer to the reforming is to submerge the reformer tubes in a bubbling fluidized bed, which allows for a higher heat transfer coefficient, lower temperature and lower emissions of NO_x, SO_x and CO than non-fluidized combustion alternatives. However, studies of fluidized bed combustion with a mixture of hydrocarbon gas and air show that combustion mainly occurs in the gas bubbles exploding at the surface of the bed. For the suggestion of submerging the reformer tubes in a fluidized bed, it is necessary to have as much heat generation as possible in the bed. To oxidize fuel also inside the bed, some or all of the bed material can be replaced by an oxygen-carrying bed material.

The heat transfer coefficient between a fluidized bed and a submerged object is well known to be high, and a large number of experimental studies have been done on the heat transfer from a fluidized bed to both single tubes and tube bundles. There are also several established heat transfer models for fluidized beds at conditions close to room temperature, but none at the high temperatures required for the steam reforming process application. The aim of this study is to experimentally determine the heat transfer coefficient between a bubbling fluidized bed and a tube at a bed temperature of 700-950°C. The experimental setup consists of a lab-scale fluidized bed reactor with a horizontal water tube positioned in the dense bed. Fine sand, coarse sand and the oxygen carrier ilmenite are all tested as bed materials.

The experiments for both fine sand and ilmenite resulted in similar values of the bed to tube heat transfer coefficient (h_o) at around 700 W/m^{2}K in the bed temperature span of 700-950°C. In the case with coarse sand, higher values ranging from 800 to 1075 W/m^{2}K were estimated. Among the investigated parameters, the bed temperature, the fluidization velocity and the particle diameter were considered to be significant. The density of the bed may also be a significant parameter, but it could not be concluded with certainty.

Keywords: heat transfer coefficient, fluidized bed heat exchanger, oxygen carrier, steam reforming

Acknowledgements

First of all we would like to thank our supervisor, PhD student Viktor Stenberg, for his support, guidance and useful feedback during the course of this thesis work. Our examiner, Associate Professor Magnus Rydén, is also acknowledged for his input and creative solutions. Finally, we would like to thank research engineers Rustan Hvitt, Jessica Bohwalli, Johannes Öhlin and Ulf Stenman for their practical help during the experimental work.

Viktor Sköldberg & Lovisa Öhrby, Gothenburg, May 2018

Contents

List of Figures

List of Tables

Nomenclature

A_i	tube inside surface area	J/(kgK)
A_o	tube outside surface area	J/(kgK)
$c_\mathrm{p,b}$	specific heat of bed	J/(kgK)
$c_\mathrm{p,g}$	specific heat of fluidization gas	J/(kgK)
d_i	tube inside diameter	m
d_o	tube outside diameter	m
d_p	bed particle diameter	m
e_b	emissivity of bed	
e_p	emissivity of bed particles	
e_s	emissivity of tube surface	
g	gravitational acceleration	$\mathrm{m/s^2}$
H_bed	height of fixed bed	m
H_tube	vertical position of horizontal tube	m
h_o	outside heat transfer coefficient	$\mathrm{W/(m^2K)}$
h_i	inside heat transfer coefficient	$\mathrm{W/(m^2K)}$
h_conv	convective component of h_o	$\mathrm{W/(m^2K)}$
h_rad	particle radiative component of h_o	$\mathrm{W/(m^2K)}$
h_w	wall conduction heat transfer coefficient	$\mathrm{W/(m^2K)}$
j_h	tube-side heat transfer factor	
k_g	thermal conductivity of fluidizing gas	W/(mK)
k_w	thermal conductivity of tube wall	W/(mK)
L	tube length in bed (bed diameter)	m
$\dot{Q}$	total heat transfer rate	W
T_b	bed temperature	K or °C
T_bulk	bulk temperature	K or °C
T_i	inside tube surface temperature	K or °C
T_in	tube inlet temperature	K or °C
T_out	tube outlet temperature	K or °C
T_s	outside tube surface temperature	K or °C
T_w	tube wall mean temperature	K or °C
U	overall heat transfer coefficient	$\mathrm{W/(m^2K)}$
u	superficial fluidization velocity	m/s
u_mf	minimum fluidization velocity	m/s
u_t	terminal velocity	m/s
$\dot{V}$	volumetric flow rate	$\mathrm{m^3/s}$

Greek letters

ΔT	temperature difference	K or °C
ΔT_{lm}	logarithmic mean temperature difference	K or °C
$\Delta \mathrm{H}^{\circ}_{298}$	standard enthalpy of formation at 298 K	kJ/mol
ϵ	bed voidage in fluidized bed	
$\epsilon_{\mathrm{fixed}}$	bed voidage in fixed bed	
μ	dynamic viscosity	Pa·s
μ_{g}	dynamic viscosity of fluidization gas	Pa·s
μ_{w}	dynamic viscosity at the wall	Pa·s
$\rho_{\mathrm{b,fixed}}$	density of fixed bed	$\mathrm{kg/m^3}$
ρ_{g}	density of fluidization gas	$\mathrm{kg/m^3}$
ρ_{p}	density of particles	$\mathrm{kg/m^3}$
σ	Stefan-Boltzmann constant ($5.67{\cdot}10^{-8}$)	$\mathrm{W/(m^2K^4)}$
ϕ_{p}	particle sphericity	

Dimensionless numbers

Ar	Archimedes number	$= \rho_{\mathrm{g}}(\rho_{\mathrm{p}}\text{-}\rho_{\mathrm{g}})\mathrm{g}d_{\mathrm{p}}^3/\mu^2$
Gz	Graetz number	$= (d/L)RePr$
Nu	Nusselt number	$= hd/k$
Pr	Prandtl number	$= c_{\mathrm{p}}\mu/k$
Re	Reynolds number	$= \rho ud/\mu$

Abbreviations

BFB	Bubbling Fluidized Bed
CLC	Chemical Looping Combustion
OCAC	Oxygen Carrier Aided Combustion
WGS	Water Gas Shift

1 Introduction

Hydrogen is a widely used raw material with a production representing around 2% of the world's primary energy demand [1]. Hydrogen is largely used in refineries for hydrocracking and desulphurization as well as in the chemical industry for the production of ammonia and fertilizers. It is also used in methanol production, the metal industry, food processing and the electronics sector [2]. Hydrogen has also been discussed as a clean and carbon-free fuel option for the future. Examples of potential renewable production technologies include biogas reforming and water splitting. However, hydrogen production from renewable sources is still expensive, which means that fossil fuels remain the most feasible source for hydrogen production in the near future [3]. Today, 96% of all hydrogen used globally comes from fossil fuels and the most common production method is steam reforming of natural gas (48% of annual hydrogen production) [1]. The steam reforming reaction is strongly endothermic and requires high temperatures (around 800-950°C) to proceed. The reforming conventionally takes place over a nickel catalyst in tubular steam reformers with heat supplied from a furnace [4]. The heat transfer is mainly radiative from flames with temperatures of around 1500°C [5].

A suggested method to improve the heat transfer to the steam reforming process is to submerge the reformer tubes in a bubbling fluidized bed [6, 7], which has a higher heat transfer coefficient both within the bed and from bed to tube. Fluidized beds are widely used for processes such as combustion and gasification [8], and they usually have a higher efficiency and lower temperature than non-fluidized alternatives. In addition, fluidized beds allow for reduced emissions of NO_x, SO_x and CO [9]. However, studies of a fluidized bed combustion with a mixture of hydrocarbon gas and air show that combustion mainly occurs in the gas bubbles exploding at the surface of the bed. The observation is that combustion only occurs in the bubble phase and when the bubbles have reached a certain size, which depends on the bed conditions [10]. For the suggestion of submerging the reformer tubes in a fluidized bed, it is necessary to have as much heat generation as possible in the bed. In order for the heat release to occur inside the bed, high temperatures (above 800°C) can be used. As the temperature increases, ignition will progress to smaller bubbles further down in the bed [10]. Another alternative is to replace some or all of the bed material with an oxygen carrier (a solid metal oxide), which has been shown in studies to oxidize hydrocarbons such as methane inside the bed even at moderate temperatures ($\sim$ 700°C) [11, 12].

This novel concept of replacing a part or all of the bed material with metal oxides as oxygen carriers is called Oxygen Carrier Aided Combustion (OCAC) and was first demonstrated in 2012 in a 12 MW circulating fluidized bed research boiler at Chalmers University of Technology. The idea of using oxygen carriers in a combustion process is already familiar from the concept of Chemical Looping Combustion

(CLC), in which oxygen carriers are recirculated between a fuel reactor, where the fuel is oxidized, and an air reactor, where the carriers are oxidized with air. Thus, the air and fuel are never mixed and the flue gases from the fuel oxidation will leave the system as a separate stream, containing CO_2 and H_2O. By simply condensing H_2O, a stream of pure CO_2 is obtained without any loss of energy for gas separation and the CO_2 can be sent to storage [13]. Regardless if the steam reformer tubes are placed in a fuel reactor in a CLC system [6] or in a single fluidized bed reactor for OCAC [7], the heat of combustion is transferred to the reformer tubes using fluidized bed technology and oxygen carriers.

The heat transfer coefficient between a fluidized bed and a submerged object is well known to be high and a large number of experimental studies have been done on the heat transfer from a fluidized bed to both single tubes and tube bundles [14]. There are also several established heat transfer models for fluidized beds at conditions close to room temperature, but none at the high temperatures required for the steam reforming process. For the investigation of the technology with fluidized bed heat transfer to submerged reformer tubes, experimental estimation of the heat transfer coefficient from bed to tube is therefore valuable.

1.1 Aim

The aim of this thesis is to determine the experimental heat transfer coefficient to the surface of a tube submerged in a bubbling fluidized bed at a temperature of 700-950°C. The aim also includes the following questions:

- How is the heat transfer coefficient affected by certain parameters and the use of different bed materials?
- Is the experimentally found heat transfer coefficient similar to theoretical values estimated with existing correlations?

1.2 Limitations

The total heat transferred to the tube can be measured but in order to determine the heat transfer coefficient from bed to tube, the heat transfer coefficient on the inside of the tube and through the tube wall is needed. These can be estimated using correlations and known tube material characteristics. Since flow in tubes is a well studied subject, it is expected that the correlations will give reliable results for the tube conditions used in this work. The experimental work is carried out in a lab-scale bubbling fluidized bed reactor with a horizontal tube positioned at a specific bed height. No other tube configurations or equipment sizes are investigated. The study is limited to three different bed materials, fine silica sand, coarse silica sand and ilmenite. The choice is due to that sand is a widely used bed material in fluidized beds and ilmenite is currently one of the most commonly used oxygen carrier materials. For simplicity, no fuel is added to the bed and the bed is fluidized by air only.

2 Theory

This chapter presents the relevant theory for this thesis. The main focus is on heat transfer applicable to flows in a tube, as well as between a bubbling fluidized bed (BFB) and a horizontal tube. A short introduction is also given to the concepts of steam reforming and Oxygen Carrier Aided Combustion (OCAC).

2.1 Steam reforming

There are different technologies for producing hydrogen and the choice depends on factors such as cost, feedstock availability and scale of production. For large-scale production, the well-established steam reforming process is the most economic and efficient technology [15]. Steam reforming is a process for converting hydrocarbons into carbon monoxide and hydrogen and it is usually followed by the water gas shift (WGS) reaction to increase the hydrogen yield by converting more of the carbon monoxide [16]. Natural gas is the preferred feedstock, but also higher hydrocarbons can be used [15]. The reactions below show the general steam reforming reaction, the steam reforming of methane and the WGS reaction [4].

$$C_nH_m + n\,H_2O \rightleftharpoons n\,CO + (n + m/2)\,H_2 \tag{1}$$

$$CH_4 + H_2O \rightleftharpoons CO + 3\,H_2 \qquad (\Delta H°_{298} = 206\ \text{kJ/mol}) \tag{2}$$

$$CO + H_2O \rightleftharpoons CO_2 + H_2 \qquad (\Delta H°_{298} = \text{-}41\ \text{kJ/mol}) \tag{3}$$

The steam reforming is reversible and strongly endothermic. Thus, in order to maximize the yield of hydrogen, it is beneficial to have a high temperature, high steam to hydrocarbon ratio and a low pressure, according to le Chatelier's principle [4]. To achieve high conversion, a catalyst is needed, normally containing nickel [16]. The catalyst is loaded in the tubes in form of a packed bed of cylindrical pellets with a large outer diameter and several holes in order to increase the surface and decrease the pressure drop [4].

The steam reforming is preferably operated with an outlet temperature of 800-950°C to achieve a high conversion. Inlet temperatures are typically 450-650°C. To supply the reforming process with heat, there are several technologies available, but the most common is to use a heated furnace with mainly radiative heat transfer to tubular steam reformers. Except for the radiant section, including the burners, there is also a convective section where the large part of heat that is not transferred to the reforming (around 40-50%) is recovered from the flue gases [4].

2.2 Fundamental heat transfer equations

The heat transfer from a hot medium to a cold medium, separated by a tube wall, can be illustrated as in Figure 2.1. The indices o, s, w and i represent outside, surface, wall and inside, respectively.

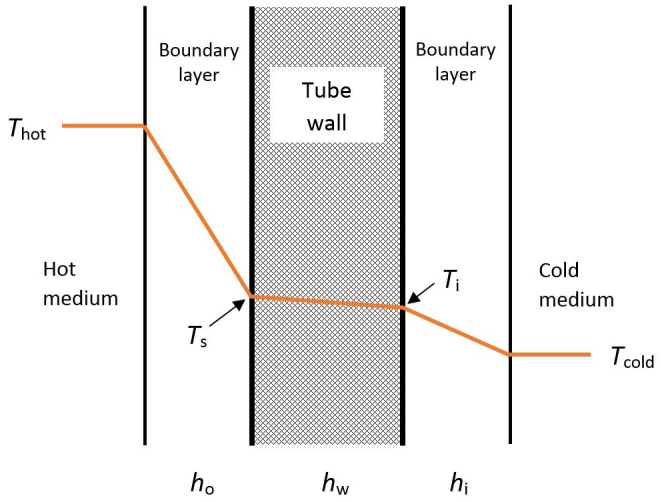

Figure 2.1: Illustration of the heat transfer from a hot medium to a cold medium. The inclination of the temperature gradient in the boundary layers and the tube wall depends on several factors and can differ between heat transfer cases.

The total heat transfer rate to the cold moving medium can be described by Equation 2.1 or 2.2.

$$\dot{Q} = \rho \dot{V} c_\mathrm{p} \Delta T \tag{2.1}$$

$$\dot{Q} = U A_\mathrm{o} \Delta T_\mathrm{lm} \tag{2.2}$$

where the overall heat transfer coefficient, U, can be expressed as in Equation 2.3 and the logarithmic mean temperature difference, ΔT_lm, is determined using Equation 2.4.

$$U = \frac{1}{\frac{1}{h_\mathrm{o}} + \frac{d_\mathrm{o} \ln(d_\mathrm{o}/d_\mathrm{i})}{2k_\mathrm{w}} + \frac{d_\mathrm{o}}{d_\mathrm{i} h_\mathrm{i}}} \tag{2.3}$$

where k_w is the thermal conductivity of the tube material.

$$\Delta T_\mathrm{lm} = \frac{\Delta T_1 - \Delta T_2}{\ln(\Delta T_1 / \Delta T_2)} \tag{2.4}$$

where ΔT_1 and ΔT_2 is the temperature difference at the inlet and outlet of a heat exchanger, respectively.

Another way to express the total heat transfer rate is to use an average expression for the conduction through the wall, Equation 2.5, or for the convection between the inner wall surface and the fluid, Equation 2.6 [17].

$$\dot{Q} = h_{\mathrm{w}} A_{\mathrm{o}} (T_{\mathrm{s}} - T_{\mathrm{i}}) \tag{2.5}$$

$$\dot{Q} = h_{\mathrm{i}} A_{\mathrm{i}} (T_{\mathrm{i}} - T_{\mathrm{bulk}}) \tag{2.6}$$

2.3 Heat transfer in tubes

The heating or cooling of a fluid flowing inside tubes is the most important convective heat transfer process in industries. Forced convection for internal flow can be described by several different correlations, often adapted to either laminar or turbulent flow, where the critical Reynolds number for tube flow is approximately 2300. Below this, the internal flow will be laminar [18]. The following two sections will present correlations for laminar and turbulent flow in tubes.

2.3.1 Laminar flow

Sieder & Tate [19] have correlated Equation 2.7 for laminar flow in tubes.

$$Nu = 1.86(RePr)^{0.33} \left(\frac{d_{\mathrm{i}}}{L}\right) \left(\frac{\mu}{\mu_{\mathrm{w}}}\right)^{0.14} \tag{2.7}$$

where μ is the dynamic viscosity at the bulk fluid temperature and μ_{w} is the dynamic viscosity at the wall.

Another approach is to use a correlation in terms of the heat transfer factor j_{h}. The j_{h} factor is shown graphically in Appendix A and enables a representation of both laminar and turbulent flow. The heat transfer correlation with j_{h} can be expressed as in Equation 2.8 [20].

$$Nu = j_{\mathrm{h}} RePr^{0.33} \left(\frac{\mu}{\mu_{\mathrm{w}}}\right)^{0.14} \tag{2.8}$$

Baehr and Stephan [21] propose a correlation of the form presented in Equation 2.9, which is specific for the *combined entry length problem* where the temperature and velocity profiles develop simultaneously. The velocity profile is said to be *fully developed* when it no longer changes with increasing length. A *thermally fully developed* condition can be reached for two different fixed tube surface conditions; uniform wall surface temperature or uniform heat flux. However, for both thermal conditions, the change in temperature compared to the entrance temperature increases with increasing length. The proposed correlation of Baehr and Stephan in Equation 2.9 is developed for the condition of constant wall surface temperature and for

laminar tube flow with $Pr \geq 0.1$.

$$Nu = \frac{\frac{3.657}{\tanh(2.264Gz^{-1/3}+1.7Gz^{-2/3})} + 0.0499Gz\tanh(Gz^{-1})}{\tanh(2.432Pr^{1/6}Gz^{-1/6})} \tag{2.9}$$

The correlation of Baehr and Stephan depends on both the diameter and length of the tube through the Graetz number:

$$Gz = \frac{d_\mathrm{i}}{L}RePr$$

Fully developed conditions (thermal and velocity) are reached for $Gz^{-1} \approx 0.05$ [17].

2.3.2 Turbulent flow

As mentioned in the last section, Equation 2.8 can also be used for turbulent flow. However, a more common heat transfer correlation for turbulent tube flow is given in Equation 2.10 [20].

$$Nu = CRe^{0.8}Pr^n\left(\frac{\mu}{\mu_\mathrm{w}}\right)^{0.14} \tag{2.10}$$

where

1. $C = 0.021$ for gases and $C = 0.023$ for non-viscous liquids
2. $n = 0.4$ if the fluid is being heated and $n = 0.3$ if the fluid is being cooled

Even though Equation 2.7-2.10 can be used for water, a more accurate estimate may be found by using Equation 2.11 [20], which is a correlation developed specifically for water with all physical properties already incorporated.

$$h_\mathrm{i} = \frac{4200(1.35 + 0.02T)u^{0.8}}{d_\mathrm{i}^{0.2}} \tag{2.11}$$

Here, T is the water temperature in °C, u is the water velocity in m/s and d_i is the tube inside diameter in mm.

2.4 Bubbling fluidized beds

Bubbling fluidized beds (BFBs) are widely used for processes such as combustion and gasification [8]. They consist of a bed usually made up of sand, fluidized by a gaseous medium such as air that is introduced through a distribution plate in the bottom of the bed together with the fuel, if it is gaseous. This creates turbulence and a good mixing of the fuel, which results in an increased conversion of hydrocarbons to energy. A BFB boiler usually have a higher efficiency, lower emissions and lower operating temperatures than non-fluidized alternatives [9].

The transition from a fixed bed to a bubbling fluidized bed occurs when the superficial gas velocity, u, becomes higher than the minimum fluidization velocity, u_{mf}. A correlation for the minimum fluidization velocity is given in Equation 2.12 [8].

$$Re_{\mathrm{mf}} = \frac{u_{\mathrm{mf}} d_{\mathrm{p}} \rho_{\mathrm{g}}}{\mu} = \sqrt{C_1^2 + C_2 Ar} - C_1 \tag{2.12}$$

where Ar is the Archimedes number,

$$Ar = \frac{\rho_{\mathrm{g}}(\rho_{\mathrm{p}} - \rho_{\mathrm{g}}) g d_{\mathrm{p}}^3}{\mu^2}$$

and C_1 and C_2 are empirical constants, for which there are several different values available in literature. One common recommendation for fine particles is to use C_1 = 33.7 and C_2 = 0.0408, found by Wen and Yu [22]. A slightly different way of determining the minimum fluidization velocity is shown in Equation 2.13 [23].

$$Re_{\mathrm{mf}} = \frac{Ar}{1400 + 5.22 Ar^{0.5}} \tag{2.13}$$

The density of the particles, ρ_{p}, can be estimated as shown below if the density of the bed at fixed condition, $\rho_{\mathrm{b,fixed}}$, is known [23].

$$\rho_{\mathrm{p}} = \frac{\rho_{\mathrm{b,fixed}}}{1 - \epsilon_{\mathrm{fixed}}}$$

When the gas velocity exceeds the minimum fluidization velocity, the pressure drop over the bed equals its weight, and the bed starts to behave similar to a liquid. A *bubble phase* made of excess gas can be formed when the gas flow increases further. The gas-solid suspension constituting the rest of the bed surrounding the bubbles is called the *emulsion phase*. Depending on the size of the bed particles, the bubbles caused by the excess gas behave differently. Fast bubbles are formed in a bed containing small particles due to the small size of the bubbles, while coarser bed particles result in slow bubbles [14].

At the surface of the dense bottom bed, a so called *splash zone* is formed, where bed material is thrown up by the rising bubbles. Most of the material returns to the dense bed, but a certain share (increases with gas velocity) travels upwards with the gas. The space above the splash zone in a BFB has a low concentration of particles and is called the *freeboard*. When the gas velocity exceeds the terminal velocity, u_{t}, some of the bed particles will be carried away and if the escaped particles are reintroduced to the bed, the term *circulating fluidized bed* is used instead [24]. The terminal velocity can be estimated with Equation 2.14 [23].

$$Re_{\mathrm{t}} = \frac{u_{\mathrm{t}} d_{\mathrm{p}} \rho_{\mathrm{g}}}{\mu} = \frac{Ar}{18 + 0.61 Ar^{0.5}} \tag{2.14}$$

2.5 Heat transfer in bubbling fluidized beds

The focus of this chapter is on the computational approach to theoretically estimate the heat transfer coefficient from bed to tube. The chapter begins by introducing the different types of models that can be used for the estimation of the heat transfer coefficient.

2.5.1 Models

The heat transfer coefficient between a fluidized bed and a heat transfer surface constitutes of convection from both gas (index gc) and particles (index pc) as well as radiation (index r). These contributions are often assumed to be additive, which means that the heat transfer coefficient becomes:

$$h_{\mathrm{o}} = h_{\mathrm{gc}} + h_{\mathrm{pc}} + h_{\mathrm{r}}$$

The convective parts are sometimes considered together as $h_{\mathrm{c}} = h_{\mathrm{gc}} + h_{\mathrm{pc}}$. For the estimation of the heat transfer coefficient, there are a number of different models that can be used. These models can be divided in the following three approaches:

1. Semiempirical models based on the mechanistic packet-renewal model
2. Comprehensive models using fluid dynamics
3. Correlations

The packet-renewal model, mentioned in approach 1, describes the heat transfer mechanism in a BFB and was developed by Mickley and Fairbanks [25]. According to the model, packets of particles are swept into contact with the heat transfer surface for a short period of time by the movements of the bubbles. The first layer of particles in contact with the surface will cool down. However, the packets are frequently replaced by new packets at bed temperature, resulting in a maintained high temperature difference between the bed particles and the surface. This heat transfer process is illustrated in Figure 2.2. To note is that the heat transfer during the short actual contact time between the first layer of particles and the surface is low, and that the main heat is transferred via conduction through the thin gas layer between the particles and the surface. Hence, the particle convection can also be called conduction.

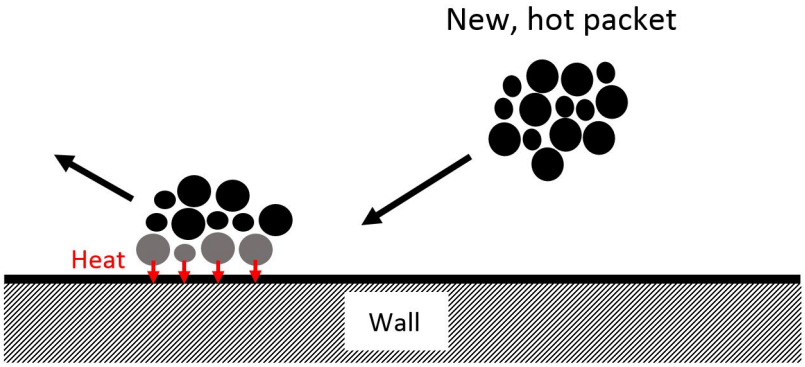

Figure 2.2: Principle of the packet-renewal heat transfer model.

The comprehensive models include the equations of energy, continuity and momentum as well as balances of chemical reactions. Even though the computer technology brings new opportunities, most of these heat transfer models for fluidized beds are simplified similar to previously developed models for BFBs [23].

The third approach, which is also the one used in this thesis work, consists of heat transfer correlations. A number of different correlations have been developed from experimental studies of the heat transfer between fluidized beds and a submerged surface. Some of these correlations are described in section 2.5.3.

2.5.2 Radiative heat transfer

The radiative heat transfer contribution can be estimated from Equation 2.15 [23].

$$h_{\mathrm{r}} = \frac{\sigma(T_{\mathrm{b}}^4 - T_{\mathrm{s}}^4)}{(\frac{1}{e_{\mathrm{b}}} + \frac{1}{e_{\mathrm{s}}} - 1)(T_{\mathrm{b}} - T_{\mathrm{s}})} \tag{2.15}$$

where σ is the Stefan-Boltzmann constant, T_{b} is the bed temperature, T_{s} is the temperature of the tube surface, e_{s} is the emissivity of the tube surface and e_{b} is the emissivity of the bed, defined below as a function of the particle emissivity, e_{p}.

$$e_{\mathrm{b}} = 0.5(1 + e_{\mathrm{p}})$$

2.5.3 Convective heat transfer correlations

There are a number of existing correlations for calculating the heat transfer from a fluidized bed to a horizontal tube. The correlations presented in this chapter have been developed for conditions close to room temperature, meaning that only the convective heat transfer is included [26]. The Nusselt number in this chapter is therefore defined as in Equation 2.16. To get a better estimation of the heat transfer at higher temperatures, the radiative contribution calculated from Equation 2.15 should also be included.

$$Nu = \frac{h_{\mathrm{c}} d_{\mathrm{o}}}{k_{\mathrm{g}}} \tag{2.16}$$

Vreedenberg [27] defines a Reynolds group, Re_{G}, as in Equation 2.17. Depending on the value of Re_{G}, Vreedenberg recommends either Equation 2.18 or Equation 2.19 for the estimation of the bed to tube heat transfer.

$$Re_{\mathrm{G}} = \frac{\rho_{\mathrm{p}} u d_{\mathrm{p}}}{\mu_{\mathrm{g}}} \tag{2.17}$$

$$Nu = 0.66 \left(\frac{\rho_{\mathrm{p}} u d_{\mathrm{o}} (1-\epsilon)}{\mu_{\mathrm{g}} \epsilon} \right)^{0.44} \left(\frac{c_{\mathrm{p,b}} \mu_{\mathrm{g}}}{k_{\mathrm{g}}} \right)^{0.3} \quad (\text{for } Re_{\mathrm{G}} < 2050) \tag{2.18}$$

$$Nu = 420 \left(\frac{\rho_{\mathrm{p}} u d_{\mathrm{o}}}{\mu_{\mathrm{g}}} \frac{\mu_{\mathrm{g}}^2}{d_{\mathrm{p}}^3 \rho_{\mathrm{p}}^2 g} \right)^{0.3} \left(\frac{c_{\mathrm{p,b}} \mu_{\mathrm{g}}}{k_{\mathrm{g}}} \right)^{0.3} \quad (\text{for } Re_{\mathrm{G}} > 2550) \tag{2.19}$$

If $2050 < Re_{\mathrm{G}} < 2550$, Vreedenberg suggests that an average of the values obtained from the two correlations can be used.

Vreedenbergs's correlation in Equation 2.19 correlates well when the bed voidage is low, according to Andeen & Glicksman [28]. But to account for the effect of a decreased particle concentration, Andeen & Glicksman modified the correlation by also including the bed voidage, see Equation 2.21 in Table 2.1. The bed voidage, ϵ, can be estimated from Equation 2.20, developed by Grewal & Saxena [26].

$$\epsilon = \frac{1}{2.1} \left[0.4 + \left[4 \left(\frac{u \mu_{\mathrm{g}}}{d_{\mathrm{p}}^2 \rho_{\mathrm{p}} \phi_{\mathrm{p}}^2 g} \right)^{0.43} \right]^{0.33} \right] \tag{2.20}$$

where ϕ_{p} is the sphericity of the bed particles.

Table 2.1 also presents a number of other existing correlations for the heat transfer between a fluidized bed and a horizontal tube. The correlations are developed using different particle sizes, materials and experimental setups, see data in Table 2.2. In general, a large range of d_{p} and rho_{p}, low values of T_{b} and large equipment sizes were used.

Table 2.1: Correlations for the heat transfer between a fluidized bed and a horizontal tube.

Reference	**Correlation**
Andeen & Glicksman [28]	$$Nu = 900(1-\epsilon)\left(\frac{\rho_\mathrm{p} u d_\mathrm{o}}{\mu_\mathrm{g}}\frac{\mu_\mathrm{g}^2}{d_\mathrm{p}^3\rho_\mathrm{p}^2 g}\right)^{0.326}\left(\frac{c_\mathrm{p,g}\mu_\mathrm{g}}{k_\mathrm{g}}\right)^{0.3} \quad (2.21)$$
Grewal & Saxena [26]	$$Nu = 47(1-\epsilon)\left(\frac{\rho_\mathrm{p} u d_\mathrm{o}}{\mu_\mathrm{g}}\frac{\mu_\mathrm{g}^2}{d_\mathrm{p}^3\rho_\mathrm{p}^2 g}\right)^{0.325}\left(\frac{\rho_\mathrm{p} c_\mathrm{p,b} d_\mathrm{o}^{3/2} g^{1/2}}{k_\mathrm{g}}\right)^{0.23}\left(\frac{c_\mathrm{p,g}\mu_\mathrm{g}}{k_\mathrm{g}}\right)^{0.3} \quad (2.22)$$
Ainshtein [29]	$$Nu = 5.76(1-\epsilon)\left(\frac{\rho_\mathrm{g} u d_\mathrm{p}}{\mu_\mathrm{g}\epsilon}\right)^{0.34}\left(\frac{c_\mathrm{p,g}\mu_\mathrm{g}}{k_\mathrm{g}}\right)^{0.33}\left(\frac{H_\mathrm{bed}}{L}\right)^{0.16}\left(\frac{d_\mathrm{o}}{d_\mathrm{p}}\right) \quad (2.23)$$
Gelperin et. al. [30]	$$Nu = 4.38\left[\frac{1}{6(1-\epsilon)}\left(\frac{\rho_\mathrm{g} u d_\mathrm{p}}{\mu_\mathrm{g}}\right)\right]^{0.32}\left(\frac{1-\epsilon}{\epsilon}\right)\left(\frac{d_\mathrm{o}}{d_\mathrm{p}}\right) \quad (2.24)$$
Genetti et al. [31]	$$Nu = 11(1-\epsilon)^{0.5}\left(1+\frac{0.2512}{(\rho_\mathrm{g} u d_\mathrm{p}/\mu_\mathrm{g})^{0.24}(d_\mathrm{p}/0.000203)^2}\right)^{-2}\left(\frac{d_\mathrm{o}}{d_\mathrm{p}}\right) \quad (2.25)$$
Ternovskaya & Korenberg [32]	$$Nu = 2.9\left[\left(\frac{1-\epsilon}{\epsilon}\right)\left(\frac{\rho_\mathrm{g} u d_\mathrm{p}}{\mu_\mathrm{g}}\right)\right]^{0.4}\left(\frac{c_\mathrm{p,g}\mu_\mathrm{g}}{k_\mathrm{g}}\right)^{0.33}\left(\frac{d_\mathrm{o}}{d_\mathrm{p}}\right) \quad (2.26)$$

Table 2.2: Data used in the development of the correlations in Table 2.1. Not found data is marked with -.

Reference	d_p	ρ_p	**Bed material**	T_b	u	**Equipment size**
	μm	kg/m^3	-	°C	m/s	H_{bed} [m] × L [m] × d_{o} [mm] × H_{tube} [m]
Vreedenberg Eq. 2.18 [27]	64-213	1600-5150	Various	40-260	0.01-0.19	1.2 × 0.565 × 17-89 × 0.85
Vreedenberg Eq. 2.19 [27]	130-353	1600-5150	Various	20-340	0.01-0.21	1.2 × 0.565 × 17-89 × 0.85
Andeen & Glicksman [28]	360-710	-	Ottawa sand	Room temp.	0.30-9.14	- × - × 19 × -
Grewal & Saxena [26]	167-504	2490-4450	Various	Room temp.	0.08-0.67	0.35 × 0.305 (square) × 13-29 × 0.21
Ainshtein [29]	160-285	-	Sand	-	-	0.35 × 0.275 × 22-30 × -
Gelperin et. al. [30]	-	-	-	-	-	-
Genetti et. al. [31]	-	-	-	-	-	-
Ternovskaya & Korenberg [32]	-	-	-	-	-	-

2.6 Oxygen Carrier Aided Combustion

Bubbling fluidized beds allow for a high heat transfer coefficient and could therefore be suitable as an option to improve the heat transfer to a steam reforming process by submerging the reformer tubes in the bed. However, studies of a fluidized bed combustion with a mixture of hydrocarbon gas and air show that combustion mainly occurs in the gas bubbles exploding at the surface of the bed. The observation is that combustion only occurs in the bubble phase and when the bubbles have reached a certain size (around 30 mm, depending on bed conditions). For the suggestion of submerging the reformer tubes in a fluidized bed, it is necessary to have the main heat generation within the bed. In order for the heat release to occur inside the bed, high temperatures (above 800°C) can be used. As the temperature increases, ignition will progress to smaller bubbles further down in the bed [10]. Another alternative is to replace some or all of the bed material with a solid metal oxide, which has been shown in studies to oxidize hydrocarbons such as CH_4 inside the bed even at moderate temperatures ($\sim$ 700°C) [11, 12]. This suggests that the heterogeneous reaction between CH_4 and metal oxides is less constrained by temperature than the homogeneous reaction between CH_4 and gaseous oxygen [33].

This concept, to partially or completely replace the sand with an oxygen-carrying bed material is called Oxygen Carrier Aided Combustion (OCAC). OCAC utilizes a metal oxide that can be reduced and oxidized through redox reactions to transport oxygen from oxygen-rich to oxygen-lean zones in the bed. Consequently, the oxygen carrier increases the contact between oxygen and fuel, which is one of the most important aspects affecting the performance of a combustion process. An enhanced mixing between oxygen and fuel results in less emissions of carbon monoxide (CO) and unburnt fuel in the flue gases, which in turn will mean a reduced need of excess air to maintain the low emissions. Reducing the demand of excess air is positive for several reasons since excess air is associated with decreased thermal efficiency, increased fuel consumption and increased capital costs and operational costs. A more even distribution of oxygen and fuel can also prevent uneven heat release in the furnace and thus, prevent the appearance of high temperature zones. The hot zones can increase the melting risk of ashes, which in turn may deposit on heat transfer surfaces with severe fouling and corrosion problems as a consequence [34]. Thus, OCAC offers the possibility to improve the combustion process from several aspects, but most importantly, it enables the main heat release to occur inside the fluidized bed.

The use of oxygen carriers in a combustion process is already familiar from the concept of Chemical Looping Combustion (CLC), in which oxygen carriers are recirculated between a fuel reactor, where the fuel is oxidized, and an air reactor, where the carriers are oxidized with air. Thus, air and fuel are never mixed and the flue gases from the fuel oxidation will leave the system as a separate stream, containing CO_2 and H_2O. By simply condensing H_2O, a stream of pure CO_2 is obtained without any loss of energy for gas separation and the CO_2 can be sent to storage [13].

There are a number of possible metals which oxide forms can be used as oxygen carriers, for instance Fe, Ni, Co, Cu, Mn and Cd [13]. It is desirable for the oxygen carrier to have low cost, good fluidization properties and sufficient reactivity and durability [34]. For OCAC, oxides of Fe or Mn are often of interest since they come from comparatively inexpensive raw materials [35]. A commonly tested oxygen carrier with acceptable performance is ilmenite - a naturally occurring iron titanium oxide [12]. Ilmenite has several possible oxidation states, where the most reduced form is $FeTiO_3$ and the most oxidized is Fe_2TiO_5 + TiO_2 [35]. An example with ilmenite as oxygen carrier for the oxidation of methane is shown in Reaction (4). The reduced form of the oxygen carrier is then re-oxidized in oxygen-rich zones according to Reaction (5). In this way, the oxygen carrier transports oxygen to oxygen-lean areas, acting as an oxygen buffer [34].

$$1/4\,CH_4 + Fe_2TiO_5 + TiO_2 \rightleftharpoons 2\,FeTiO_3 + 1/4\,CO_2 + 1/2\,H_2O \tag{4}$$

$$2\,FeTiO_3 + 1/2\,O_2 \rightleftharpoons Fe_2TiO_5 + TiO_2 \tag{5}$$

3 Method

This chapter begins by describing the preparations needed for the experimental work. This is followed by a presentation of the experimental setup and explanation of how the experiments were conducted. The final section describes how the theoretical estimation of the heat transfer coefficient from bed to tube (h_o) was carried out using existing correlations.

3.1 Preparations

In order to perform the experimental part of the thesis work, an investigation was done regarding which fluid medium that would be most suitable to use in the tube. Both water and air were considered as possible options in the available lab setup. At first, a range of volumetric flow rates ($\dot{V}$) for both water and air, respectively, was established for values of h_o between 100 and 1000 W/(m^{2}K). The iterative procedure presented in Figure 3.1 was used for the flow estimation.

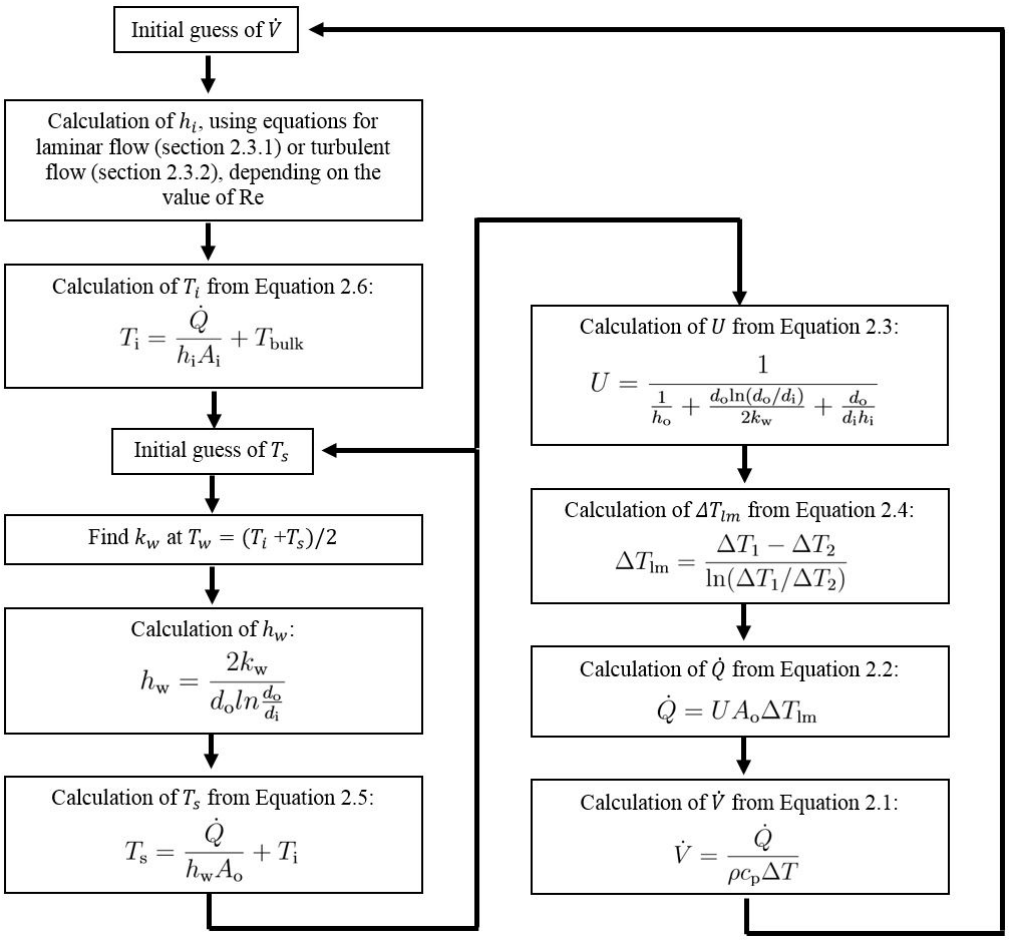

Figure 3.1: Iteration procedure for the estimation of $\dot{V}$.

A second calculation, presented in Figure 3.2, was established in order to determine h_o. This path was used for the initial sensitivity analysis and also later, when calculating the experimental h_o from measured data.

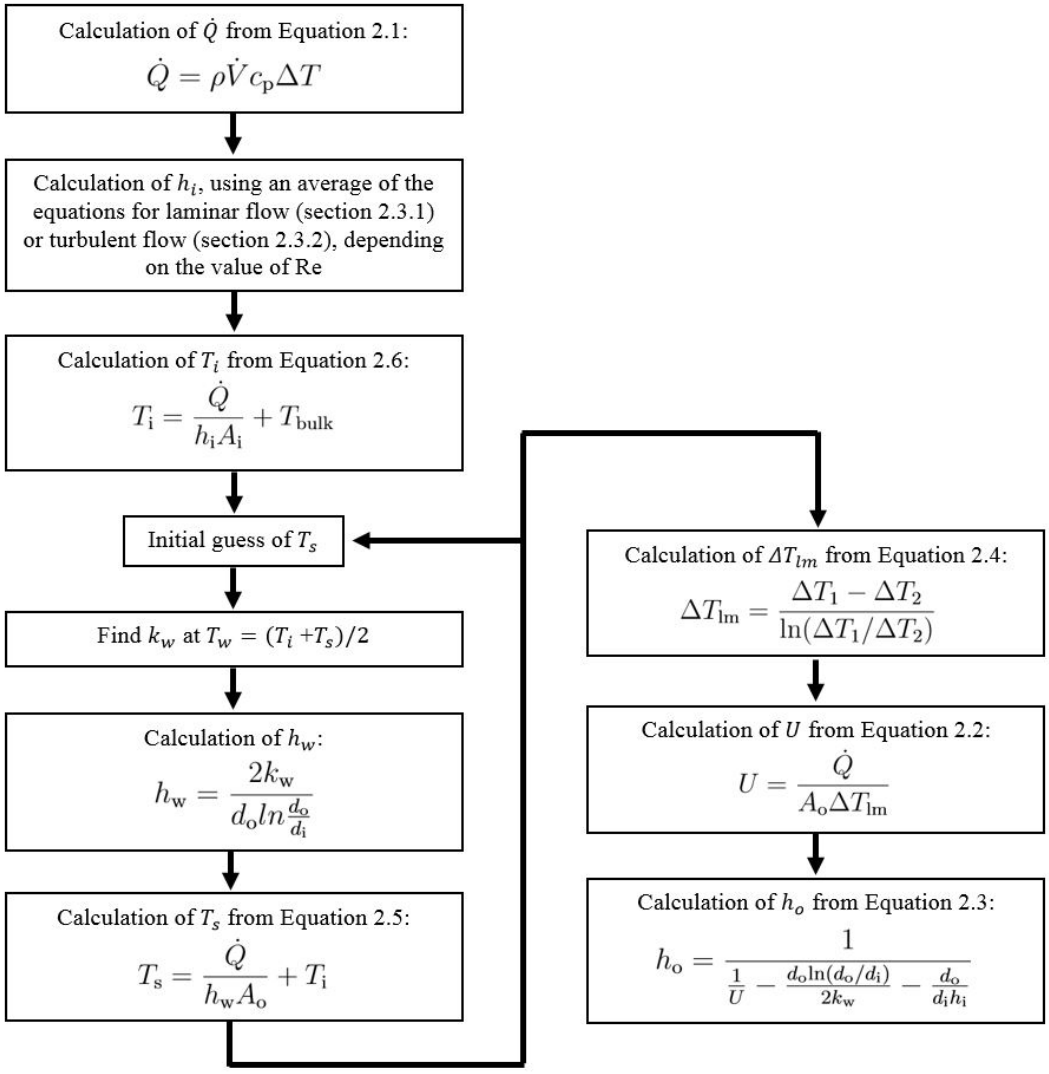

Figure 3.2: Procedure for calculating h_o.

In the calculations, properties of the tube wall and the fluid are evaluated at the mean temperatures of the wall and fluid, respectively. Furthermore, since the mixing in fluidized beds is fast and results in close to isothermal reactor conditions, the temperature was assumed to be constant throughout the bed.

By assuming a base case for the operation conditions, a preliminary sensitivity analysis was done to see what effects errors in measurements may have on the estimated h_o. The analyzed parameters were the volumetric flow rate ($\dot{V}$), the inlet temperature of the fluid (T_{in}) and the temperature of the bed (T_b). Based on the sensitivity analysis, water was found to be the most suitable tube-side fluid in this case and hence, only water was used in the continued work. The reasoning behind

this decision is further explained in chapter 4.1.

Another important matter to consider before the experimental work is the velocity of the fluidization air, since the bed needs to be operated within the range of a bubbling fluidized bed ($u_{\mathrm{mf}} < u < u_{\mathrm{t}}$). Thus, the minimum fluidization velocity (u_{mf}) was estimated using both Equation 2.12 and 2.13 for comparison, and the terminal velocity (u_{t}) was estimated using Equation 2.14.

3.2 Experimental setup

The equipment consisted of a lab-scale bubbling fluidized bed reactor with a single horizontal tube made of Inconel alloy 600, positioned at half of the bed height. See an approximate illustration of the reactor in Figure 3.3. A simple representation of the heat transfer was used, with bed material fluidized by air only and without the presence of fuel in the reactor.

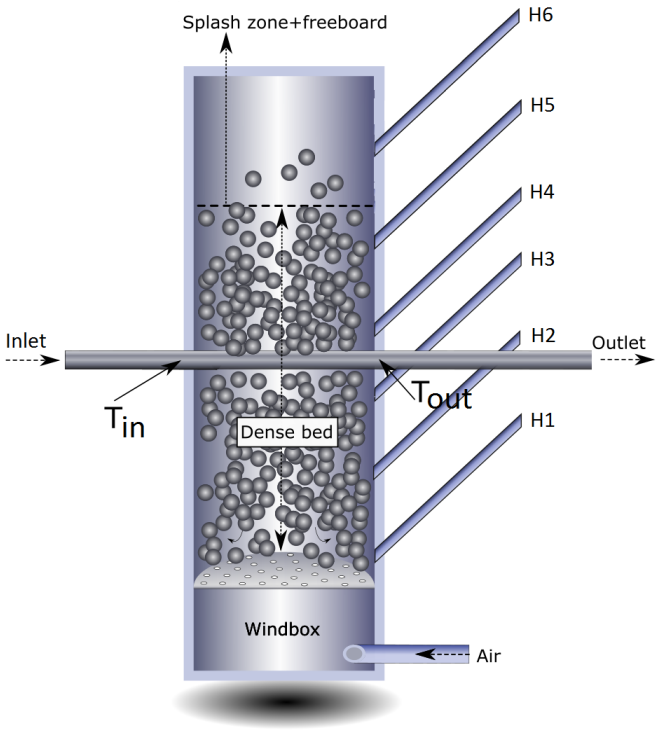

Figure 3.3: Approximate illustration of the fluidized bed reactor.

A number of positions for pressure measurements (H1-H6 in Figure 3.3) were situated along the height of the bed reactor, together with a single bed temperature measurement (H3 in Figure 3.3) close to the horizontal tube. Temperature measurements were also located at the inlet and outlet of the tube. Detailed dimensions of the reactor setup are presented in Table 3.1.

Table 3.1: Dimensions of the reactor setup.

	Variable	Value	Unit
Bed diameter (= length of tube in bed)	L	77.92	mm
Height of fixed bed	H_{bed}	150	mm
Vertical position of horizontal tube	H_{tube}	75	mm
Tube inside diameter	d_{i}	4	mm
Tube outside diameter	d_{o}	6	mm
Distribution plate, hole diameter	d_{hole}	0.8	mm
Distribution plate, number of holes	N_{hole}	61	

In order to reach the desired bed temperatures, heat was supplied by an electrically heated furnace in which the reactor was placed, see Figure 3.4.

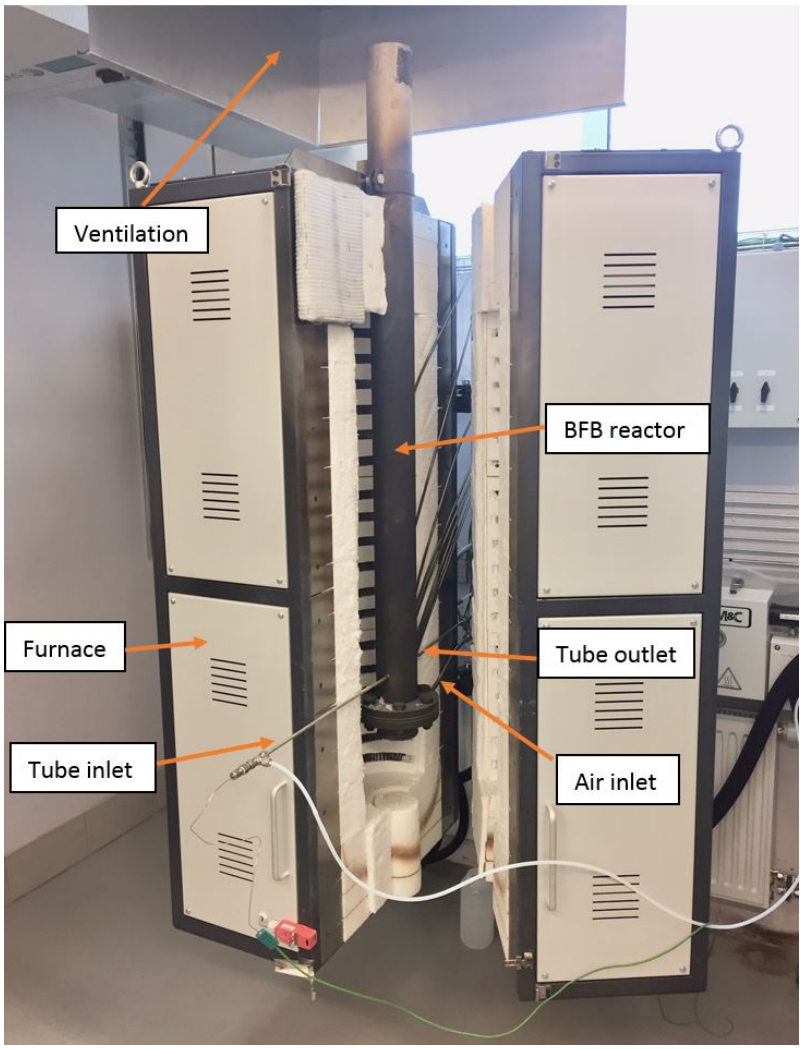

Figure 3.4: Picture of the fluidized bed reactor placed inside the electric furnace.

Figure 3.5 shows an illustration of the entire experimental setup. The feed to the tube was water, connected from a water tap with a hose and a valve to ensure an even and adjustable flow. As can be seen in the figure, the water tube had to be bent at the outlet from the reactor in order for the tube to fit around the instruments measuring the pressure and temperature in the bed. Consequently, the water outlet temperature had to be measured at a position around 2 cm from the reactor wall. To estimate the effect of this additional length at the outlet, a small experiment was done where the thermocouple measuring the inlet temperature was pulled out 2 cm from the reactor wall.

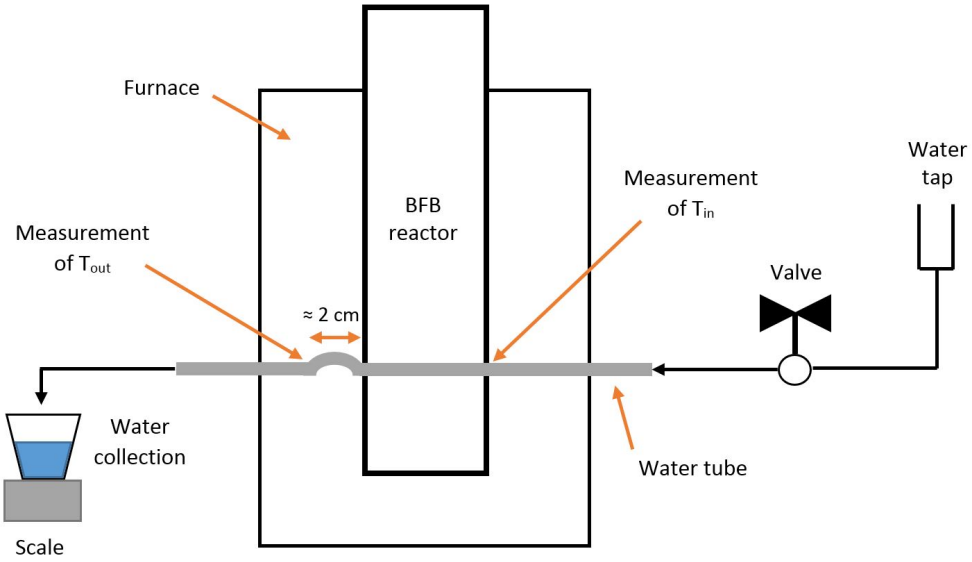

Figure 3.5: Illustration of the experimental setup.

As bed material, fine sand, coarse sand and ilmenite were tested separately in order to study the effects and significance of using different particle sizes and different materials. Before the experiments, fine sand and ilmenite were sieved to a size range of 90-212 μm, and the coarse sand was delivered in the range of 90-500 μm. The weighted mean diameter as well as bulk density (using poured bulk density technique) were determined for each material, see Table 3.2. Photos of sand and ilmenite can be seen in Figure 3.6.

Table 3.2: Bulk density and mean particle diameter of sand and ilmenite.

	Fine sand	**Coarse sand**	**Ilmenite**	**Unit**
Bulk density (poured)	1424	1505	2253	kg/m^3
Weighted mean diameter	128	267	150	μm

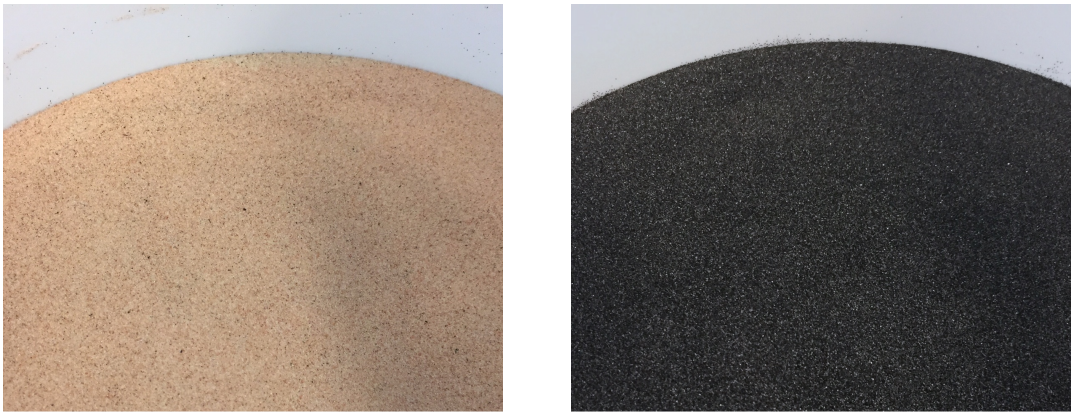

(a) Silica sand (b) Ilmenite

Figure 3.6: The bed material.

It should also be pointed out that there are several differences between a commercial steam reformer and the experimental setup used in this thesis work. Scale is an obvious example, where industrial sized plants can have reformers with an outside tube diameter of 150 mm and a tube length of up to 13 m. Furthermore, tube arrangements in a commercial steam reformer usually consists of multiple tubes positioned vertically in the furnace [4].

A horizontal tube was used in this study since a vertical tube configuration is much more difficult to construct. The value of the heat transfer coefficient may differ between the two tube configurations, but for the experimental setup used in this study, they are expected to be close to equal. This expectation is suggested by correction factors, which can be used to correlate the heat transfer coefficient between horizontal and vertical tubes. The correction factors are close to one for the tube and reactor dimensions used in this study [8].

3.3 Experimental procedure

Parameters that could be adjusted were $\dot{V}$, u and the set temperature of the electrically heated furnace, which in turn controlled T_{b}. The first step was to find an experimentally feasible range for $\dot{V}$ at the chosen base case values of T_{b} and u, used in the initial investigation in section 3.1. The minimum $\dot{V}$ was chosen as to avoid boiling and the unstable operation occurring close to boiling, which was observed for lower values of $\dot{V}$ in the way that the flow started to go back and forth in the tube, due to partly boiling and condensation of the water. To maintain an even flow, it was observed that water outlet temperatures of maximum around 75°C were favorable, which in turn defined the minimum $\dot{V}$. The maximum $\dot{V}$ depended on the maximum capacity of the hose and the valve. Each tested $\dot{V}$ was calibrated by adjusting the valve and then measured by collecting the water exiting the reactor in a bucket during a time period of up to 60 seconds. The collected water was weighed and divided by the density (based on the mean water temperature in the tube) to obtain $\dot{V}$.

Secondly, the water flow was varied within the found flow range while keeping the other parameters constant at the base case values, in order to study its effect on h_o. Each experimental set of temperatures and pressures was taken as the average of the data collected during 300 seconds. During this runtime and due to a maximum limit of the scale, 3-5 water flow measurements were done.

When the water flow analysis was finished, a base case value for $\dot{V}$ was chosen. This value is not necessarily the same as in the theoretical investigation in section 3.1, since that value was only used for a first screening of tube medium choice and was not sure to be feasible in reality, due to the outlet temperature constraint (sub-boiling). The outlet temperature could not be fully predicted in the initial analysis, since both the value of h_o and the increase in water temperature were unknown.

Continuing with the base case, u was varied within a range between the minimum fluidization velocity and below the terminal velocity. Then T_b was varied between 700 and 950°C. However, after evaluation, this range was expanded to include also values between 400 and 700°C since it could be of interest to see the effect on h_o at a broader bed temperature span.

Last, pressure data from the experiments when varying u was composed in a graph to see how well the transition from fixed to fluidized bed agrees with the theoretical estimation of u_{mf}.

This experimental procedure was done for each of the three bed materials, except the determination of water flow range which was only done for fine sand. The same flow range was used for all three cases.

3.4 Theoretical estimation of h_o using existing correlations

In section 2.5, a number of existing correlations for the heat transfer between a fluidized bed and a horizontal tube were presented. Even though none of them are developed for the high temperature range, same equipment size etc. as in this study, a comparative analysis was done to investigate eventual trends and similarities between the correlations and the experimental results obtained in this work.

The comparison was done by using the same temperatures and water flow rates as measured in the experiments, as well as the measured bulk density and mean diameter of the bed materials. The correlations also need a few other bed material properties. Approximate values for these are taken from literature and are presented in Table 3.3. The emissivity of ilmenite particles was not found in literature and was assumed to be 0.9. Another property that had to be assumed was the bed voidage in a fixed bed, for which a reasonable value is 0.4 [23]. Furthermore, the emissivity of the tube wall surface was assumed to be approximately 0.9 [36].

Table 3.3: Material properties of sand and ilmenite.

	Variable	**Sand**	**Ilmenite**	**Unit**	**Reference** sand/ilmenite
Emissivity of particles	e_{p}	0.9	0.9		[17]
Specific heat capacity of bed	$c_{\mathrm{p,b}}$	800	900	J/(kgK)	[17] / [37]
Sphericity of particles	ϕ_{p}	0.80	0.77		[8, 24] / [38]

4 Results

This chapter begins by introducing the results from the preliminary investigation, including choice of tube medium and theoretical estimations of internal tube flow rate, measurement error sensitivity and minimum fluidization velocity. The second part presents the experimental results from the studies of different bed temperatures, fluidization velocities, tube flow rates and bed materials. In the third part, the experimental results are compared with existing heat transfer correlations.

4.1 Initial theoretical investigation

Approximate values of a suitable fluid flow ($\dot{V}$) in the tube were estimated to be 1-7 ml/s for water and 300-1300 ml/s for air, considering a bed to tube heat transfer coefficient (h_o) of 100-1000 W/m^{2}K and a bed temperature (T_b) of 825°C. A wide range of h_o was used since at this stage in the study, the real value of h_o was unknown. For the sensitivity analysis, the values in Table 4.1 were used as a theoretical base case. Important to note is that this base case is made of chosen parameters and only for selection of tube medium and estimation of the sensitivity to measurement errors in the experiments. Thus, it is not an experimentally validated set of parameters.

Table 4.1: Base case for the initial sensitivity analysis.

	Variable	**Water**	**Air**	**Unit**
Bed temperature	T_b	825	825	°C
Inlet temperature	T_{in}	20	20	°C
Outlet temperature	T_{out}	60	250	°C
Volumetric flow rate	$\dot{V}$	4.0	800	ml/s

In Figure 4.1, air is used as tube side fluid and the resulting h_i and h_o are plotted against the estimated range of $\dot{V}$ for air. Since the air flow is turbulent, there are only two equations (2.8 and 2.10) that can be used to calculate h_i, viewed in the figure as two separate lines. It is clear that the two lines coincide poorly and thus, that it is very hard to predict h_o when using air in the tube.

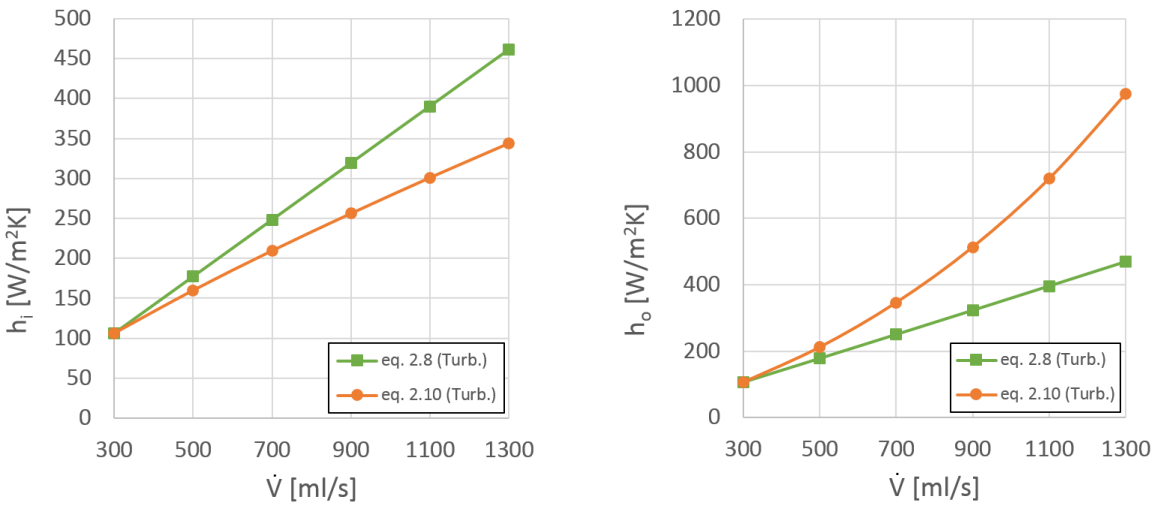

Figure 4.1: Values of h_i (left) and h_o (right) for the estimated flow range of air.

Similar to Figure 4.1, Figure 4.2 shows h_i and h_o plotted against $\dot{V}$ when using water in the tube, but for a smaller range of $\dot{V}$. When comparing Figure 4.1 and 4.2, two important differences can be observed. First, the correlations of h_i agree much better for the use of water in the tube. Secondly, the value of h_i is a lot higher for water than for air. A high value of h_i is desired in this study since eventual changes of h_i will have a smaller impact on h_o. Small values of h_i imply that h_o will be much more sensitive to the accuracy of the estimated h_i. Based on these insights, water was chosen as tube side medium for the continued work.

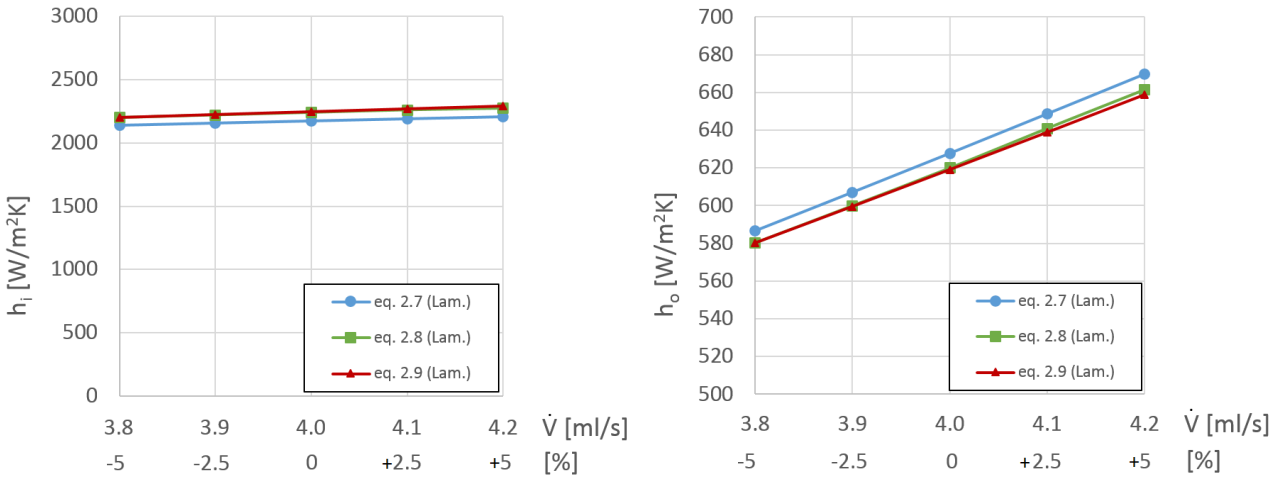

Figure 4.2: Estimated change in h_i (left) and h_o (right) for small errors in water flow measurement.

Figure 4.2 is plotted with deviations of $\dot{V}$ in percentage added on the x-axis to give an understanding of how small errors in the measurement of $\dot{V}$ may affect the result of h_o. For example, an error in the measured flow of $\pm$ 5% is estimated to give an

error in h_o of around 40 W/m^{2}K, corresponding to a deviation of about 6% from the base case value.

The water case was further analyzed by also looking at how errors in the measurement of T_{in} and T_b could affect h_o, see Figure 4.3. An error of ± 5% in the measured T_{in} is estimated to give an error in h_o of around 20 W/m^{2}K (∼ 3% from the base case value). Similarly, a deviation of ± 5% in the measured T_b may cause an error in h_o of around 40 W/m^{2}K (∼ 6% from the base case value). When considering these numbers, it seems like the measurement of $\dot{V}$ and T_b are the most sensitive to errors. However, a 5% error in the measured T_b corresponds to about 42 °C, while a 5% error in T_{in} corresponds to only 1°C. In that sense, T_{in} may be even more sensitive than T_b, depending on the point of view.

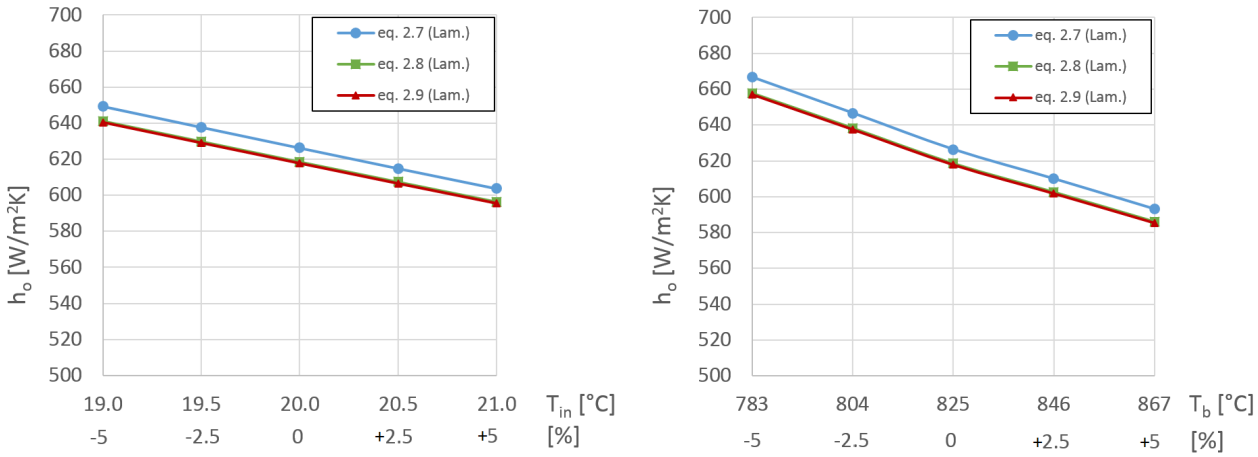

Figure 4.3: Estimated change in h_o for small errors in water inlet temperature (left) and bed temperature (right).

The theoretically estimated fluidization velocity range for each bed material is presented in Table 4.2. For the minimum fluidization velocity (u_{mf}), the table presents the largest of the two values obtained by Equation 2.12 and 2.13.

Table 4.2: Theoretical fluidization velocity range (u_{mf} - u_t) at a bed temperature of 825°C.

Bed material	u_{mf} - u_t	**Unit**
Fine sand	0.006 - 0.43	m/s
Coarse sand	0.027 - 1.68	m/s
Ilmenite	0.013 - 0.89	m/s

4.2 Experimental results

As described in section 3.3, experiments were conducted by varying one of the three examined parameters at a time while trying to keep the other two constant at the chosen experimental base case values, shown in Table 4.3.

Table 4.3: Base case for the experimental analysis.

	Variable	**Value**	**Unit**
Bed temperature	T_b	825	°C
Fluidization velocity	u	0.15	m/s
Water flow rate	$\dot{V}$	20	ml/s

For T_b, a base case value of 825°C was used, which is in the middle of the initially conceived span of 700-950°C. The fluidization velocity (u) was varied between the theoretically estimated u_mf and 0.3 m/s, which made 0.15 m/s a suitable base case value. For $\dot{V}$, the lowest value that could be used without reaching boiling conditions in the tube was observed to be around 6 ml/s, which is a significantly higher value than the one found in the theoretical investigation. Consequently, a different base case value for $\dot{V}$ was used when performing the experiments. The maximum capacity of the valve was around 40 ml/s, which made 20 ml/s a reasonable choice as a base case value of $\dot{V}$.

The experimental results of varying $\dot{V}$, T_b and u for the three examined bed materials are shown in Figure 4.4, 4.5 and 4.6, for which the corresponding numerical data can be found in Appendix B. Figure 4.4, with varied $\dot{V}$, shows that the results for fine sand and ilmenite are very similar and at a fairly constant value of h_o around 700 W/m^{2}K. For the coarse sand, the result shows higher values of h_o, around 900 to 1050 W/m^{2}K.

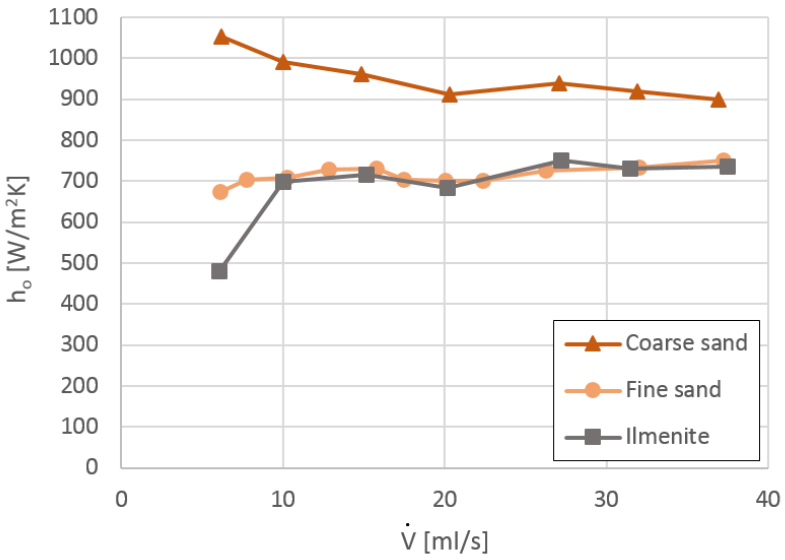

Figure 4.4: Experimentally found heat transfer coefficients at different water flow rates.

The results of varying T_b can be seen in Figure 4.5. The general trend for all bed materials is a steady increase in h_o with increasing temperature. However, above 800°C the trend for both fine sand and ilmenite ceases to increase, reaching a value of around 700 W/m^{2}K. For coarse sand, the trend continues to increase up to around 1075 W/m^{2}K. An additional line, representing only the radiative contribution to h_o, is also plotted in Figure 4.5. It is represented by a single graph since the radiation was almost identical for all three bed materials.

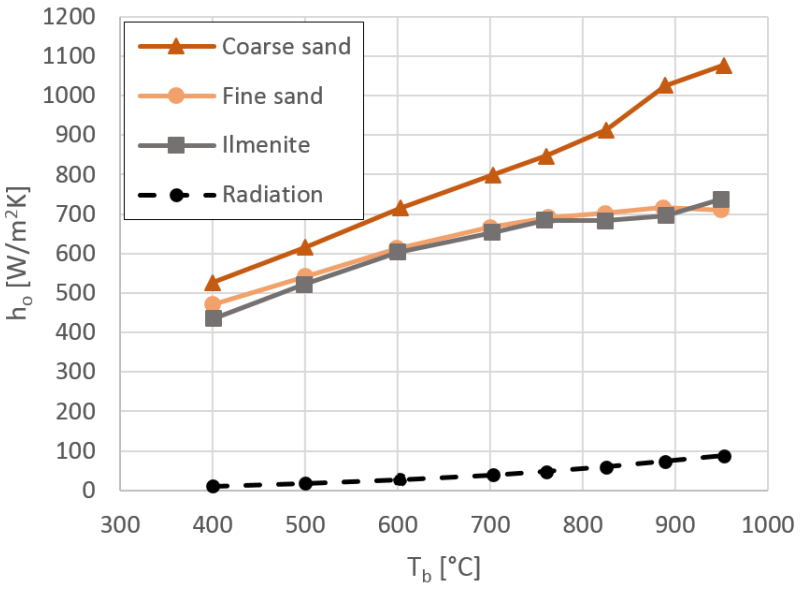

Figure 4.5: Experimentally found heat transfer coefficients at different bed temperatures, including a representation of only the radiative contribution to h_o.

Figure 4.6 shows the experimentally found h_o for increasing values of u. As in the previous two figures, all three bed materials show a relatively similar trend, with results for fine sand and ilmenite very close to each other and coarse sand at higher values of h_o. Specific for the variation of u is a rapid increase in h_o in the beginning of the increasing fluidization, before the trend stabilizes at around 700 W/m^{2}K for fine sand and ilmenite, or 900 W/m^{2}K for coarse sand.

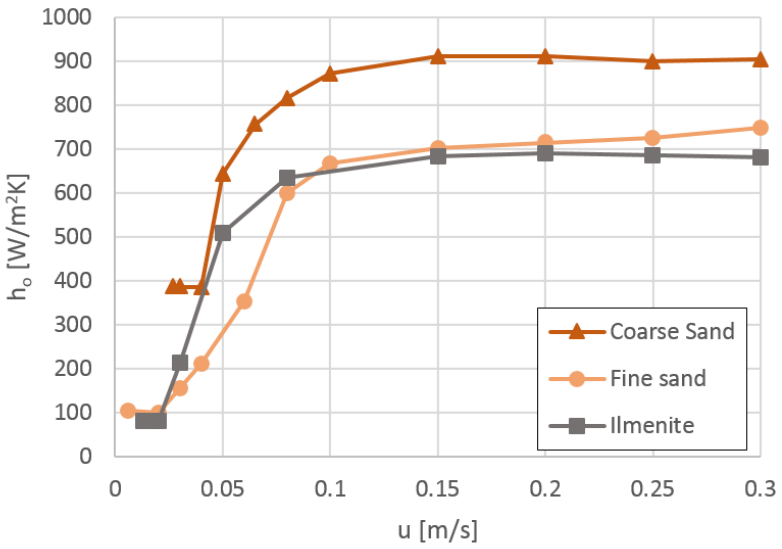

Figure 4.6: Experimentally found heat transfer coefficients at different fluidization velocities.

The result from the experiment where the thermocouple measuring T_{in} was pulled out 2 cm from the reactor inlet is presented in Table 4.4. The table shows that the increase in water temperature difference (ΔT_w) for the two different positions was small (0.19°C).

Table 4.4: Water temperature difference between inlet and outlet (ΔT_w) when measuring T_{in} at two different positions.

Variable	$\boldsymbol{T_{in}}$ **measured at inlet**	$\boldsymbol{T_{in}}$ **measured 2 cm from inlet**	**Unit**
T_b	508.0	511.3	°C
ΔT_w	14.73	14.92	°C

Pressure data from six different heights in the reactor (see H1-H6 in Figure 3.3) was collected for each analysis of increasing u from fixed to fluidized bed. The result for all three bed materials is presented in Figure 4.7. For all three cases, the pressure rises steeply in the first increase of gas velocity and then soon becomes more constant.

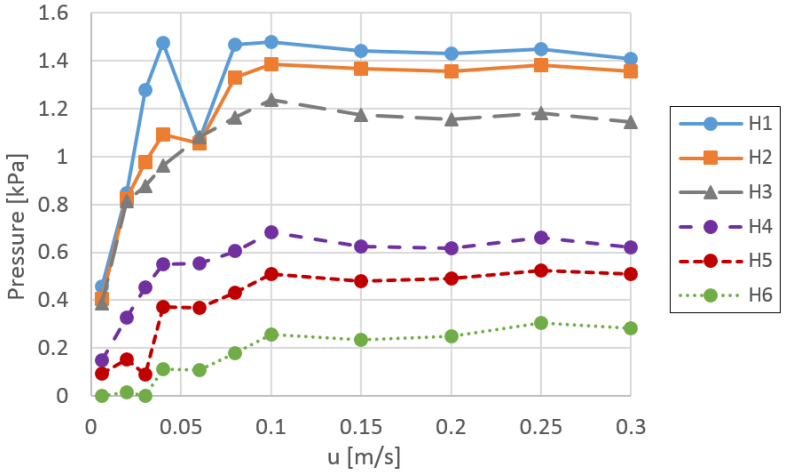

(a) Fine sand

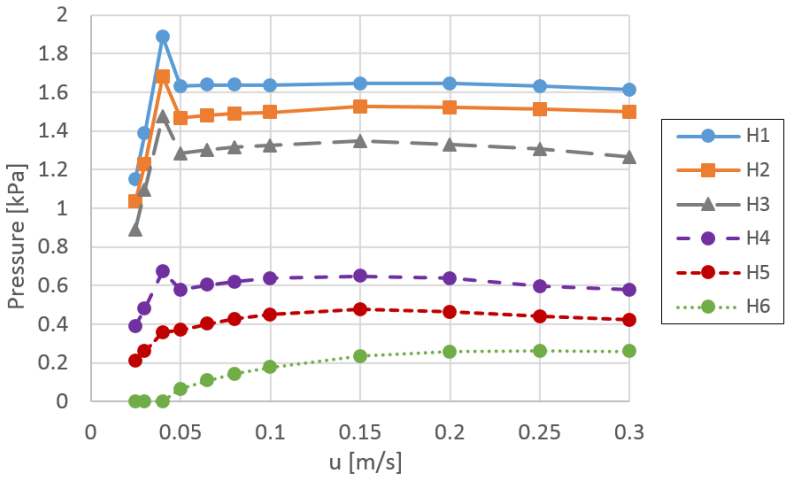

(b) Coarse sand

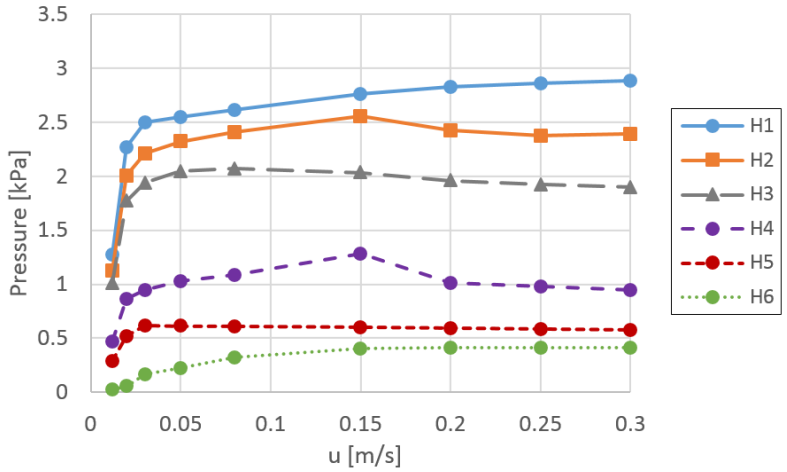

(c) Ilmenite

Figure 4.7: The measured gauge pressure at different heights in the reactor when increasing the fluidization velocity from the theoretically estimated u_{mf} to 0.3 m/s.

4.3 Comparison with correlations

The results of the theoretical estimation of h_o at different values of T_b and for all three bed materials, using the eight heat transfer correlations presented in chapter 2.5.3, are shown in Figure 4.8. The radiative heat transfer contribution (Equation 2.15) is included. Furthermore, the water temperatures, water flow rate and equipment dimensions used in the correlations are the same as in the experiments.

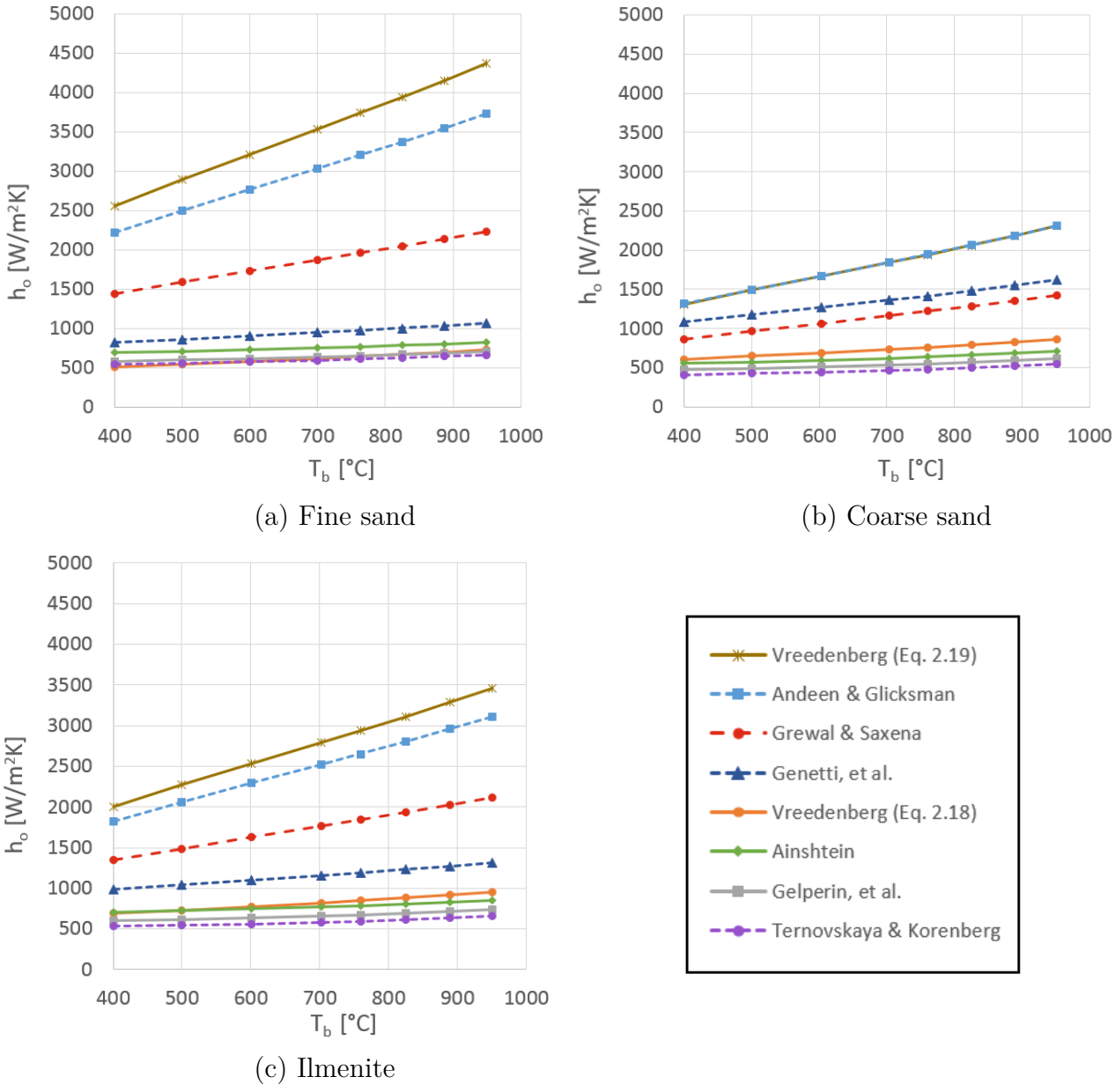

(a) Fine sand

(b) Coarse sand

(c) Ilmenite

Figure 4.8: Theoretically estimated h_o for all three bed materials, using existing heat transfer correlations.

As can be seen in the figure, the correlations give very diverse values of h_o in the range of 500-4400 W/m^{2}K. Four of the eight correlations are consistently between 500-1000 W/m^{2}K for the three studied bed materials. These four are plotted together with the experimental results in Figure 4.9 in order to get a good comparison between correlations and experiments. Important to remember is that all correlations are developed at different conditions, seen in Table 2.2, and that their validity for comparison with the experimental results in this study can be discussed.

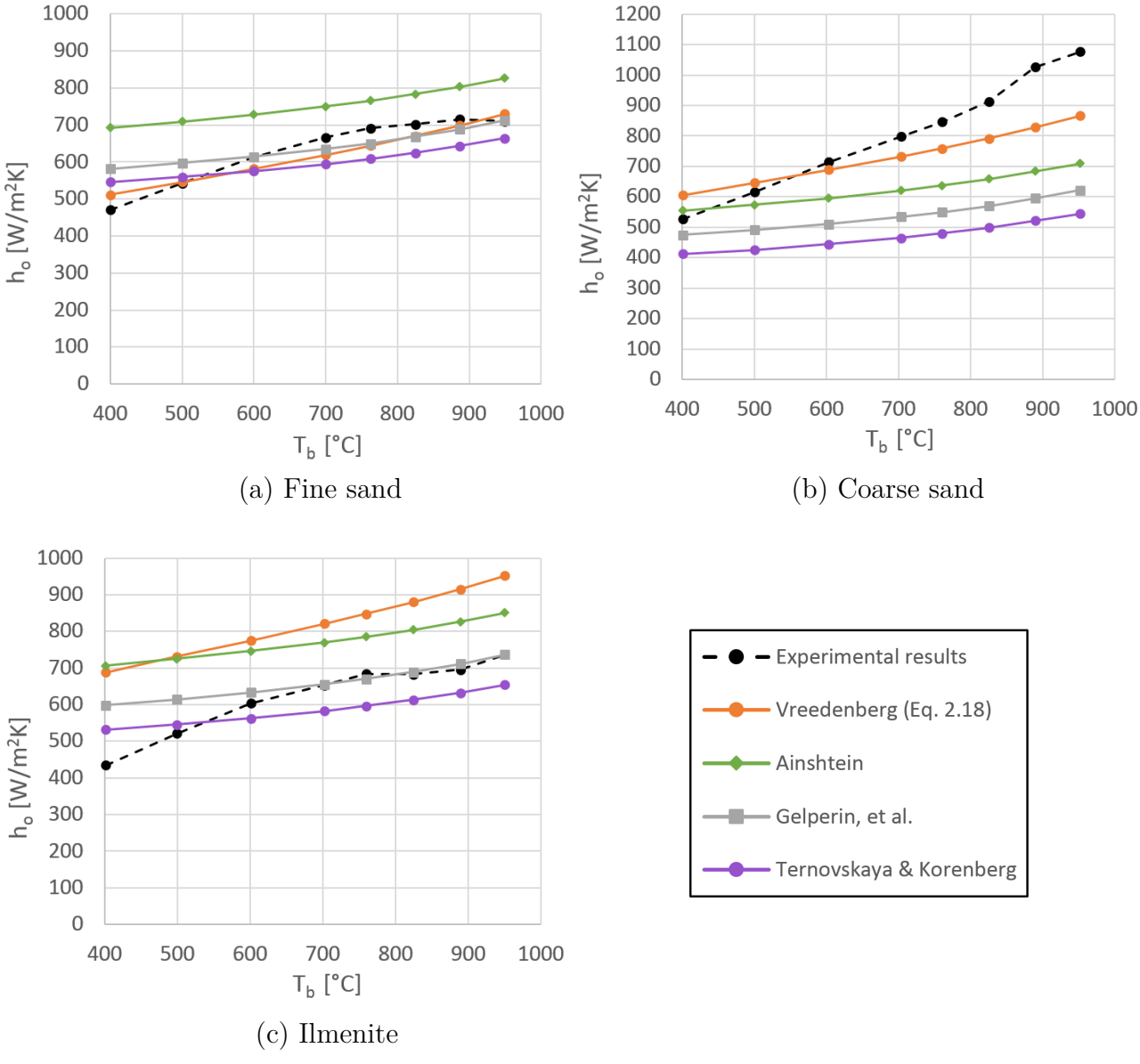

(a) Fine sand

(b) Coarse sand

(c) Ilmenite

Figure 4.9: Comparison between experimental results and theoretically estimated values of h_o from selected correlations.

5 Discussion

This chapter is divided into the three main parts; initial theoretical investigation, experimental results and comparison with correlations.

5.1 Initial theoretical investigation

Of the two available tube side fluid alternatives, water and air, water was concluded to be the most suitable choice in this study due to two reasons:

- The values of h_{i} for air differed significantly between the correlations
- The values of h_{i} for air are much lower than for water

Consequently, errors in the tube side measurements will have a greater impact on h_{o} if using air.

The parameters that were investigated further before the experiments were $\dot{V}$, T_{in} and T_{b}. The sensitivity analysis of these parameters showed that accuracy in the measurements is desired, but in this study, it could not be concluded exactly how sensitive each parameter is in the experiments. One reason for this is that the estimated error impact of T_{in} and $\dot{V}$ depends on the temperature rise of the water through the tube and the size of the water flow, respectively, and these values were not the same in the initial investigation and in the experimental work.

5.2 Experimental results

Parameters that were considered to be of interest for the experimental study of h_{o} in this thesis were the bed temperature (T_{b}), fluidization velocity (u) and properties of the bed material, such as density (ρ_{b}) and particle diameter (d_{p}). All of these are related to the conditions of the bed and are relatively easy to change. The flow rate of water ($\dot{V}$) was also considered to be of interest, since varying $\dot{V}$ was expected to not have a significant affect on h_{o} and thus, it could indicate whether the experimental procedure has been well performed or not. As expected, the result of varying $\dot{V}$ showed that h_{o} stayed fairly constant over the whole range, which is positive and justifies the procedure.

Overall, the results of the tests with fine sand and ilmenite matched each other well in all of the conducted experiments, while coarse sand consistently achieved higher values of h_{o} compared to the other two bed materials. This indicates that an increased particle size results in an increased value of h_{o}. A possible explanation can be found by considering the packet-renewal model, described in chapter 2.5.1. It is possible that large particles are cooled less before the packet is replaced by a new

one, meaning that a higher average temperature gradient is achieved compared to a case with small particles. This would then result in a higher value of h_o. Regarding the particle density, the trend is more unclear. Although ilmenite has a much higher density than fine sand, they show similar trends of h_o. This would indicate that density is not affecting h_o. However, ilmenite also has a slightly larger mean particle diameter than fine sand, which should enhance h_o for ilmenite. The fact that the trends for ilmenite and sand are similar therefore suggests that a higher density might lead to a decreased value of h_o.

When increasing T_b from 400°C, h_o steadily started to increase in all three bed material cases, which is expected due to the increased radiative heat transfer from the hot bed material to the tube. However, h_o for both fine sand and ilmenite ceased to increase at around 700 W/m^{2}K in the range 760-950°C. The reason for this is not known.

The last parameter that was varied for each bed material was u. At the lowest values of u, a few constant values of h_o were observed. This suggests that the real u_{mf} is higher than the one determined theoretically, or more specifically, two to four times higher. This can be further confirmed by looking at how the gauge pressure first increases when u was increased, which indicates that the bed is fixed. However, when u exceeds the actual u_{mf}, h_o rises steeply. Once the bed is properly fluidized, h_o stays fairly constant when increasing u further. Thus, to obtain a high value of h_o, it is necessary to have a high enough value of u. A summary of the discussions of all investigated parameters is presented in Table 5.1.

Table 5.1: Summarized evaluation of the investigated parameters.

Parameter	**Important for h_o?**	**Trend of h_o when increasing parameter value**
$\dot{V}$	No	$\rightarrow$
T_b	Yes	$\nearrow$
u	Yes	$\nearrow \quad \rightarrow$
d_p	Yes	$\nearrow$
ρ_b	Maybe	not clear

Other potentially interesting parameters that were not investigated in this study could be the position of the tube in the bed, the size of the tube and reactor as well as the number of holes and hole diameter in the gas distribution plate.

5.2.1 Possible sources of error

There are some possible sources of error in the experimental determination of h_o, mainly related to uncertain accuracy of the measured $\dot{V}$, where timing is critical. Another source of error is due to the tube bend at the outlet of the reactor, since the thermocouple measuring the water temperature could not be placed directly at the outlet. It was instead measured around 2 cm away from the reactor wall, meaning that the furnace may heat the water further after leaving the reactor and thus, affect the measured outlet temperature. However, since the space outside the reactor is taken up by stationary air, the heat transfer from the furnace to the tube is mainly radiative. This means that the additional contribution is expected to be very small compared to the heat transfer inside the fluidized bed reactor. This hypothesis was justified by the experiment with the adjusted measurement position of T_{in}, which showed that the additional distance corresponding to the length of the tube bend at the outlet should only have a negligible impact on the result.

5.2.2 Recommendations for further research

Further research of h_o is necessary to strengthen the results and to confirm the trends for different operating conditions and the use of different bed materials. Examples of parameters that would be especially interesting to investigate are a greater variety of particle sizes, other bed materials and other fluidization gases than air. It can also be of interest to see how much an introduction of fuel in the reactor would affect the heat transfer. For the steam reforming purpose, tests with a typical fuel composition for this process could be of particular interest.

Other parameters that could be interesting to study are, as mentioned before, the position of the tube in the bed, the size of the tube and reactor as well as the number of holes and hole diameter in the gas distribution plate.

5.3 Comparison with correlations

Some of the investigated correlations give a very high estimation of h_o, while others tend to stay between 500-1000 W/m^{2}K. It is clear that none of the correlations perfectly describes the experimental trends for h_o found in this study, which was not expected either since the correlations were developed using different bed particle sizes, densities, equipment sizes etc. The correlations were rather seen as an interesting way of comparing the experimental result with theoretically estimated values and to understand the difficulty of estimating h_o for a certain fluidized bed reactor setup.

The result found with correlations has several possible sources of error, such as uncertainty regarding the property values found in literature and the uncertain accuracy of the measured mean particle diameter. Another example is the measurement of the bulk density, which depends on the assumed fixed bed voidage of 0.4.

6 Conclusion

All experiments with fine sand and ilmenite showed very similar results of the heat transfer coefficient from bed to tube (h_o), with values around 700 W/m^{2}K in the bed temperature span of 700-950°C. The corresponding experiments with coarse sand consistently achieved higher results of h_o than the other two bed materials, with values ranging from 800 to 1075 W/m^{2}K in the same temperature span. Parameters that were found to be significant for the value of h_o were the bed temperature, the fluidization velocity and the particle diameter. The density of the bed may also be a significant parameter, but it could not be concluded with certainty.

None of the existing correlations could perfectly describe the experimental result of h_o, which is explained by the fact that the correlations were developed using different bed properties and in general larger equipment than the one used in this study. Nevertheless, the correlations were seen as an interesting way of comparing the experimental result with theoretically estimated values. The comparisons also illustrated the difficulty of estimating h_o for a certain fluidized bed reactor setup.

For further research of the heat transfer from a high temperature fluidized bed to a submerged tube, it would be interesting to investigate a greater variety of particle sizes, other bed materials, other fluidization gases and the introduction of fuel in the reactor. For the steam reforming purpose, tests with a typical fuel composition for this process could be of particular interest. It could also be relevant to investigate the effect of using different positions of the tube in the bed and larger dimensions of the tube and reactor.

References

[1] da Silva Veras T, Mozer TS, da Costa Rubim Messeder dos Santos D, da Silva César A. Hydrogen: Trends, production and characterization of the main process worldwide. International Journal of Hydrogen Energy. 2017;42(4):2018 – 2033.

[2] IEA Hydrogen. Global Trends and Outlook for Hydrogen [Internet]; 2017. [Cited 2018-05-22]. Available from: `http://ieahydrogen.org/pdfs/Global-Outlook-and-Trends-for-Hydrogen_Dec2017_WEB.aspx`.

[3] LeValley TL, Richard AR, Fan M. The progress in water gas shift and steam reforming hydrogen production technologies – A review. International Journal of Hydrogen Energy. 2014;39(30):16983 – 17000.

[4] Rostrup-Nielsen J, Rostrup-Nielsen T. Large-scale Hydrogen Production. Topsøe Technologies; 2001.

[5] Guiberti TF, Garnier C, Scouflaire P, Caudal J, Labegorre B, Schuller T, et al. Experimental and numerical analysis of non-catalytic partial oxidation and steam reforming of $CH_4/O_2/N_2/H_2O$ mixtures including the impact of radiative heat losses. International Journal of Hydrogen Production. 2016;41(20):8616 – 8626.

[6] Rydén M. Hydrogen production with carbon dioxide capture by reforming of natural gas using chemical-looping technologies [Licentiate thesis]. Chalmers University of Technology; 2006.

[7] Stenberg V, Rydén M, Mattisson T, Lyngfelt A. Exploring novel hydrogen production processes by integration of steam methane reforming with chemical-looping combustion (CLC-SMR) and oxygen carrier aided combustion (OCAC-SMR). International Journal of Greenhouse Gas Control. 2018;74:28 – 39.

[8] Basu P. Combustion and Gasification in Fluidized Beds. Boca Raton, Florida: Taylor & Francis Group; 2006.

[9] Pascual Peña JA. Bubbling Fluidized Beds, When to Use This Technology. Industrial Fluidization South Africa. 2011;p. 57 – 66.

[10] Dennis JS, Hayhurst AN, Mackley IG. The ignition and combustion of propane/air mixtures in a fluidised bed. Nineteenth Symposium (International) on Combustion. 1982;19(1):1205 – 1212.

[11] Chandeesingh DR, Hayhurst AN. The combustion of a fuel-rich mixture of methane and air in a bubbling fluidized bed of silica sand at 700°C and also

with particles of Fe_2O_3 or Fe present. Fuel. 2014;127:169 – 177.

[12] Adanez J, Abad A, Garcia-Labiano F, Gayan P, de Diego LF. Progress in Chemical-Looping Combustion and Reforming technologies. Progress in Energy and Combustion Science. 2012;38(2):215 – 282.

[13] Lyngfelt A, Leckner B, Mattisson T. A fluidized-bed combustion process with inherent CO_2 separation; application of chemical-looping combustion. Chemical Engineering Science. 2001;56(10):3101 – 3113.

[14] Kunii D, Levenspiel O. Fluidization Engineering. 2nd ed. Boston, Massachusetts: Butterworth-Heinemann; 1991.

[15] Rostrup-Nielsen JR, Sehested J. Steam Reforming for Hydrogen - The Process and the Mechanism. Fuel Chemistry Division Preprints. 2013;48(1):218 – 219.

[16] Trane R, Dahl S, Skjøth-Rasmussen MS, Jensen AD. Catalytic steam reforming of bio-oil. International Journal of Hydrogen Energy. 2012;37(8):6447 – 6472.

[17] Incropera FP, Dewitt DP, Bergman TL, Lavine AS. Principles of heat and mass transfer, 7th ed. Singapore: John Wiley & Sons; 2013.

[18] Welty JR, Rorrer GL, Foster DG. Fundamentals of Momentum, Heat and Mass Transfer, 6th ed. Singapore: John Wiley & Sons; 2015.

[19] Sieder FN, Tate GE. Heat Transfer and Pressure Drop of Liquids in Tubes. Industrial Engineering Chemistry. 1936;28(12):1429 – 1435.

[20] Sinnott RK. Coulson & Richardson's Chemical Engineering, Vol 6, 4th ed. Oxford: Elsevier Butterworth-Heinemann; 2005.

[21] Baehr HD, Stephan K. Heat and Mass Transfer, 3rd ed. Berlin, Germany: Springer; 2011.

[22] Wen CY, Yu YH. A generalised method for predicting the minimum fluidization velocity. American Institute of Chemical Engineers. 1966;12(3):610 – 612.

[23] Leckner B. Heat and Mass Transfer. In: Michaelides EE, Crowe CT, Schwarzkopf JD, editors. Multiphase Flow Handbook. 2nd ed. Boca Raton, Florida: Taylor & Francis Group; 2016. p. 994 – 1028.

[24] Leckner B. Short Course on Fluidization Applied to Fuel Conversion. Gothenburg, Sweden; 2017. Lecture material, Chalmers University of Technology.

[25] Mickley HS, Fairbanks DF. Mechanism of heat transfer to fluidized beds. American Institute of Chemical Engineers. 1955;1(3):374 – 384.

[26] Grewal NS, Saxena SC. Heat transfer between a horizontal tube and a gas-solid fluidized bed. Int J Heat Mass Transfer. 1980;6:1505 – 1519.

[27] Vreedenberg HA. Heat transfer between a fluidized bed and a horizontal tube.

Chemical Engineering Science. 1958;9(1):52 – 60.

[28] Andeen BR, Glicksman LR, Rohsenow WM. Improvement of the environmental and economic characteristics of cooling towers. Part I of II: Heat rejection from horizontal tubes to shallow fluidized beds. MIT Energy Lab; 1974.

[29] Ainshtein VG. An Investigation of Heat Transfer Process Between Fluidized Beds and Single Tubes Submerged in Fluidized Beds;. In Grewal NS, Saxena SC Effect of Surface Roughness on Heat Transfer from Horizontal Immersed Tubes in a Fluidized Bed. Journal of Heat Transfer. 1979;101(3):397 - 403.

[30] Gelperin NI, Kruglikov VY, Ainshtein VG. Heat Transfer between a Fluidized Bed and a Surface;. In Grewal NS, Saxena SC. Effect of Surface Roughness on Heat Transfer from Horizontal Immersed Tubes in a Fluidized Bed. Journal of Heat Transfer. 1979;101(3):397 - 403.

[31] Genetti WE, Schmall RA, Grimmett ES. The Effect of Tube Orientation on Heat Transfer With Bare and Finned Tubes in a Fluidized Bed;. In Grewal NS, Saxena SC. Effect of Surface Roughness on Heat Transfer from Horizontal Immersed Tubes in a Fluidized Bed. Journal of Heat Transfer. 1979;101(3):397 - 403.

[32] Ternovskaya AN, Korenberg YG. Fluidized Bed Furnaces and Heat Exchangers;. In Grewal NS, Saxena SC. Effect of Surface Roughness on Heat Transfer from Horizontal Immersed Tubes in a Fluidized Bed. Journal of Heat Transfer. 1979;101(3):397 - 403.

[33] Rydén M, Hanning M, Corcoran A, Lind F. Oxygen Carrier Aided Combustion (OCAC) of Wood Chips in a Semi-Commercial Circulating Fluidized Bed Boiler Using Manganese Ore as Bed Material. Applied Sciences. 2016;6(11):1 – 19.

[34] Thunman H, Lind F, Breitholtz C, Berguerand N, Seemann M. Using an oxygen-carrier as bed material for combustion of biomass in a 12 MW_{th} circulating fluidized-bed boiler. Fuel. 2013;113:300 – 309.

[35] Wang P, Leion H, Yang H. Oxygen-Carrier-Aided Combustion in a Bench-Scale Fluidized Bed. Energy & Fuels. 2017;31(6):6463 – 6471.

[36] Metals S. Inconel alloy 600 [pamphlet on the Internet]; 2008. [Cited 2018-03-06]. Available from: `http://www.specialmetals.com/assets/smc/documents/alloys/inconel/inconel-alloy-600.pdf`.

[37] Anovitz LM, Treiman AH, Essene EJ, Hemingway BS, Westrum jr EF, Wall VJ, et al. The heat-capacity of ilmenite and phase equilibria in the system Fe-Ti-O. Geochimica et Cosmochimica Acta. 1985;49:2027 – 2040.

[38] Luckos A, den Hoed P. Fluidization and flow regimes of titaniferous solids. Ind Eng Chem Res. 2004;43:5645 – 5652.

A Heat transfer factor j_h

The heat transfer factor, which can be used with Equation 2.8 to estimate the tube-side heat transfer coefficient [20].

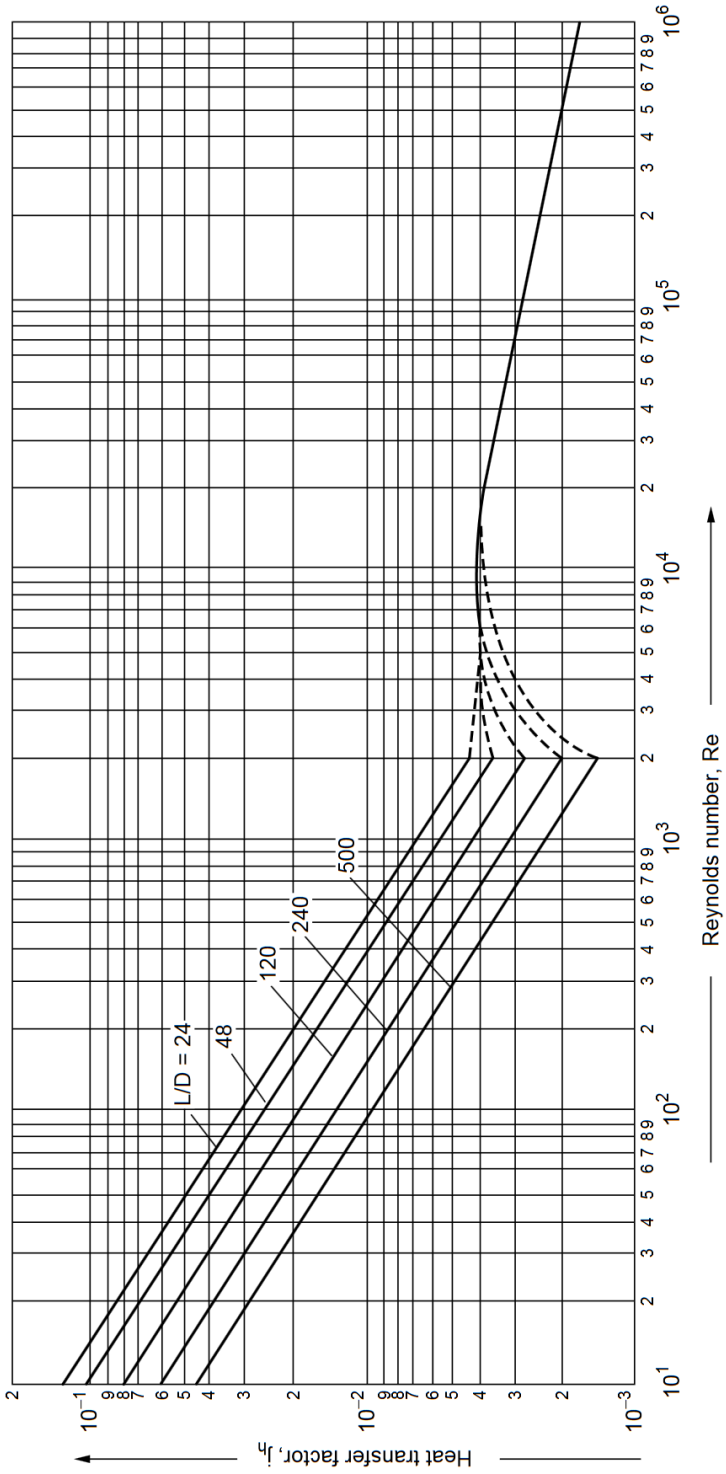

B Experimental data

The experimental result in numerical tables. Table B.1, B.2 and B.3 present the result from varying the water flow rate ($\dot{V}$), the bed temperature (T_b) and the fluidization velocity (u), respectively.

Table B.1: Numerical result of varying $\dot{V}$ for all three bed materials.

Fine sand						
$\dot{V}$ [ml/s]	T_{in} [°C]	T_{out} [°C]	T_b [°C]	Re	h_i [W/m^{2}K]	h_o [W/m^{2}K]
6.13	34.82	66.33	824.76	3534	4229.8	674.4
7.76	29.86	56.31	825.94	3922	4804.7	702.6
10.27	22.04	42.78	826.23	4277	5473.2	709.2
12.86	18.78	36.06	823.72	4898	6259.9	727.3
15.77	17.2	31.69	825.49	5696	7165.0	731.4
17.51	17.61	30.36	824.52	6273	7756.2	703.0
20.07	15.14	26.37	824.68	6795	8385.1	701.8
22.39	15.88	26.04	824.04	7606	9169.3	701.7
26.25	12.65	21.68	824.28	8346	10024.5	726.3
32.03	12.82	20.39	825.17	10087	11688.7	732.5
37.24	10.31	17.02	825.49	11149	12789.6	750.0

Coarse sand						
$\dot{V}$ [ml/s]	T_{in} [°C]	T_{out} [°C]	T_b [°C]	Re	h_i [W/m^{2}K]	h_o [W/m^{2}K]
6.19	23.26	66.03	825.90	3218	4063.9	1054.2
9.99	18.61	45.99	823.57	4155	5351.6	990.9
14.87	15.68	34.71	825.39	5442	6884.1	960.9
20.29	13.97	27.84	825.72	6884	8468.1	912.8
27.08	13.15	24.08	824.07	8828	10428.3	939.4
31.89	13.19	22.44	824.80	10254	11791.0	919.6
36.91	12.48	20.41	824.19	11591	13070.9	900.5

Ilmenite						
$\dot{V}$ [ml/s]	T_{in} [°C]	T_{out} [°C]	T_b [°C]	Re	h_i [W/m^{2}K]	h_o [W/m^{2}K]
6.05	43.16	67.62	826.00	3787	4350.1	480.9
10.03	24.97	45.95	825.40	4416	5521.8	699.5
15.14	19.56	34.32	824.37	5717	7101.5	715.0
20.16	16.16	27.1	824.63	6928	8485.0	683.2
27.23	17.74	26.74	823.86	9461	10858.9	750.8
31.48	14.12	21.79	823.88	10146	11685.6	730.5
37.49	13.13	19.68	824.68	11766	13230.5	735.1

Table B.2: Numerical result of varying T_b for all three bed materials.

Fine sand						
T_b [°C]	T_{in} [°C]	T_{out} [°C]	$\dot{V}$ [ml/s]	Re	h_i [W/m^{2}K]	h_o [W/m^{2}K]
399.79	17.41	22.15	20.30682	6757	8381.2	470.4
500.56	12.7	18.96	20.11717	6251	7992.7	542.4
599.11	12.33	20.13	20.30584	6353	8085.8	612.7
700.05	13.39	22.83	20.16149	6516	8195.0	665.9
762.93	13.8	24.02	20.54767	6734	8387.5	691.5
824.68	15.14	26.37	20.07486	6795	8385.1	701.8
886.72	15.31	27.2	20.42819	6975	8544.9	715.4
949.46	16.92	29.38	20.48046	7230	8722.1	710.3

Coarse sand						
T_b [°C]	T_{in} [°C]	T_{out} [°C]	$\dot{V}$ [ml/s]	Re	h_i [W/m^{2}K]	h_o [W/m^{2}K]
400.28	17.82	23.12	20.06	6756	8356.6	526.5
499.99	13.78	20.72	20.26	6452	8155.9	615.8
603.03	13.57	22.62	20.04	6476	8154.6	714.6
703.18	13.84	24.82	20.30	6702	8341.9	798.6
760.57	13.99	26.28	20.17	6754	8366.0	845.9
825.72	13.97	27.84	20.29	6884	8468.1	912.8
889.32	14.18	30.43	20.18	7018	8548.6	1025.5
952.32	14.86	32.64	20.29	7239	8706.8	1076.4

Ilmenite						
T_b [°C]	T_{in} [°C]	T_{out} [°C]	$\dot{V}$ [ml/s]	Re	h_i [W/m^{2}K]	h_o [W/m^{2}K]
401.11	11.67	16.15	20.09	6041	7827.6	434.9
499.03	12.19	18.22	20.14	6192	7949.9	521.6
600.56	13.16	20.92	20.18	6401	8111.4	603.5
702.31	14.61	23.91	20.21	6663	8305.2	653.7
759.06	15.38	25.71	20.05	6761	8359.0	684.4
824.63	16.16	27.1	20.16	6928	8485.0	683.2
889.68	18.5	30.28	20.20	7291	8731.2	695.6
950.19	19.5	32.53	20.24	7517	8878.8	736.8

Table B.3: Numerical result of varying u for all three bed materials.

Fine sand							
u [m/s]	T_{in} [°C]	T_{out} [°C]	T_b [°C]	$\dot{V}$ [ml/s]	Re	h_i [W/m^{2}K]	h_o [W/m^{2}K]
0.006	15.10	17.05	825.37	19.91	6214	7947.8	105.0
0.01	14.39	16.41	824.09	19.96	6156	7907.6	109.3
0.02	14.87	16.70	823.07	20.35	6317	8061.5	100.7
0.03	14.64	17.49	825.22	20.03	6250	7985.3	156.5
0.04	14.80	18.63	824.96	19.87	6269	7986.6	211.8
0.05	15.34	20.35	827.27	20.11	6470	8156.4	284.8
0.06	14.83	20.94	826.35	20.11	6476	8160.9	353.5
0.08	15.57	25.26	825.95	20.41	6867	8468.5	601.1
0.10	14.58	25.19	825.86	20.40	6800	8420.5	667.6
0.15	15.14	26.37	824.68	20.07	6795	8385.1	701.8
0.20	15.01	26.50	824.29	19.92	6742	8333.2	715.4
0.25	15.09	26.54	825.05	20.30	6879	8466.6	726.5
0.30	15.39	27.35	826.25	19.96	6831	8398.9	749.9

Coarse sand							
u [m/s]	T_{in} [°C]	T_{out} [°C]	T_b [°C]	$\dot{V}$ [ml/s]	Re	h_i [W/m^{2}K]	h_o [W/m^{2}K]
0.027	14.28	20.88	824.97	20.30	6500	8195.1	388.9
0.03	14.27	20.88	824.76	20.18	6463	8157.5	387.4
0.04	14.34	20.95	825.68	20.14	6457	8149.9	386.2
0.05	14.48	25.03	824.25	19.80	6585	8211.2	643.7
0.065	14.18	26.19	827.34	20.05	6720	8330.9	757.1
0.08	14.15	26.89	821.07	20.03	6752	8350.8	816.8
0.10	14.43	27.98	826.21	19.99	6820	8394.0	872.4
0.15	13.97	27.84	825.72	20.29	6884	8468.1	912.8
0.20	19.31	33.31	827.80	20.20	7544	8891.9	911.7
0.25	17.80	31.68	824.00	20.05	7279	8705.4	899.9
0.30	15.42	29.36	823.52	19.98	6961	8489.5	904.4

Ilmenite							
u [m/s]	T_{in} [°C]	T_{out} [°C]	T_b [°C]	$\dot{V}$ [ml/s]	Re	h_i [W/m^{2}K]	h_o [W/m^{2}K]
0.013	15.78	17.28	825.22	20.11	6325	8048.7	81.1
0.02	15.60	17.09	825.66	20.19	6330	8059.3	80.8
0.03	16.54	20.37	824.57	19.97	6492	8159.7	212.9
0.05	16.08	24.64	824.29	19.94	6703	8308.4	510.2
0.08	16.39	26.75	827.32	20.00	6867	8427.0	634.1
0.15	16.16	27.10	824.63	20.16	6928	8485.0	683.2
0.20	17.48	28.63	827.09	19.99	7045	8546.3	689.8
0.25	17.11	28.05	825.95	20.29	7093	8610.6	686.7
0.30	16.95	27.86	823.69	20.14	7019	8545.2	680.9